ROS are evolutionary conserved cell-to-cell signals

Yosef Fichman[1], Linda Rowland[2], Melvin J. Oliver[1], and Ron Mittler[1,3,*]

[1]Division of Plant Sciences and Technology, College of Agriculture Food and Natural Resources and Interdisciplinary Plant Group, Christopher S. Bond Life Sciences Center University of Missouri. 1201 Rollins St, Columbia, MO 65201, USA.

[2]Department of Surgery, University of Missouri School of Medicine, Christopher S. Bond Life Sciences Center, University of Missouri, 1201 Rollins St, Columbia, MO 65201, USA

Running title: Evolution of cell-to-cell ROS signaling

***Corresponding author:** Ron Mittler (mittlerr@missouri.edu)

Key words: Reactive oxygen species, hydrogen peroxide, evolution, signal transduction, heart, plant, algae, mice, amoeba, cancer.

Abstract

Cell-to-cell communication is fundamental to multicellular organisms and unicellular organisms living in a microbiome. A unique cell-to-cell communication mechanism that uses reactive oxygen species (ROS) as a signal (termed the 'ROS wave') was recently identified in flowering plants. Here we report that a ROS-mediated cell-to-cell signaling process, like the ROS wave, can be found in ferns, mosses, unicellular algae, amoeba, mammalian cells, and isolated hearts. We further show that this process can be triggered by a localized stress treatment or H_2O_2 application and blocked by inhibition of NADPH oxidases, and that in unicellular algae, it communicates important stress-response signals between cells. Taken together, our findings suggest that cell-to-cell ROS signaling evolved before unicellular and multicellular organisms diverged. The finding of a ROS wave-like signaling process in mammalian cells further contributes to our understanding of different diseases and could impact the development of new drugs that target cancer or heart disease.

Introduction

Cells communicate with each other in many ways. The exchange of signals between cells is thought to have evolved as part of a mechanism to control cell density (*e.g.,* quorum sensing; QS)[1,2], and/or as part of a response mechanism to changes in environmental conditions (*e.g.,* in cells living in a biofilm)[3,4]. Cell-to-cell communication can occur between cells of the same species or organism (*e.g.,* in a multicellular organism)[5,6], as well as between cells of different organisms (*e.g.,* during interactions of cells with different bacterial or fungal pathogens)[7,8]. Two of the most conserved cell-to-cell signaling pathways are paracrine, secretion of signals that are perceived by neighboring cells, and juxtacrine, communication between cells connected via tunneling nano tubes, gap junctions, or plasmodesmata[9–11]. Examples of these signaling pathways can be found in archaea, bacteria, unicellular eukaryotes, and multicellular organisms[12]. With the evolution of the vascular and nervous systems, paracrine signaling was extended to endocrine signaling, the release of signals into the bloodstream, and paracrine and juxtacrine signaling began to contribute to long distance signaling as part of electrical and chemical synapses[5,6]. In addition, autocrine signaling evolved as a mechanism for cells to regulate their own function[13]. Cell-to-cell signaling therefore plays an important role in coordinating the developmental and environmental responses of groups of neighboring cells, as well as cells that are remotely connected via blood vessels or neurons.

In vascular plants, that lack true nervous and circulatory systems, local cell-to-cell communication is primarily mediated by paracrine (via the apoplast and cell wall) and juxtacrine (via plasmodesmata; PD) signaling, while long distance signaling is mediated through the vascular system (phloem and xylem vessels, as well as their associated cells)[14,15]. Among the key signals exchanged by plant cells are different metabolites, small RNA and peptide molecules, hormones, calcium, volatile compounds, hydraulic pressure signals, membrane potential changes (electric signals), and reactive oxygen species (ROS)[14–18]. A unique cell-to-cell signaling mechanism discovered in plants is the 'ROS wave'[19–21]. The ROS wave is an auto-propagating cell-to-cell signaling pathway in which the initiating cell activates extracellular (apoplastic) ROS production via respiratory burst oxidase homologs [RBOHs; the plant homologs of NADPH oxidases (NOXs) of mammalian cells][19–21]. The ROS produced by this cell is then sensed by neighboring cells and triggers in them a similar enhanced ROS production process, resulting in the activation of a cascade or wave of cell-to-cell 'enhanced ROS production state' that spreads from the initiating cells/tissues over long distances, sometimes spanning the entire length of the plant[20,21]. The ROS wave was also recently shown to spread from one plant to another, when plants physically touch each other and conditions are sufficiently humid[22]. In addition to plasma membrane-localized RBOHs, the ROS wave requires the function of PD-localized proteins, different calcium channels, calcium signaling proteins, phytochrome B, and the plasma membrane (PM)-localized apoplastic ROS receptor H_2O_2-induced Ca^{2+} increases 1 (HPCA1) protein[21,23,24].

Numerous studies have shown that the ROS wave is linked to cell-to-cell calcium and electric signaling and that it is required for plant acclimation to stress (*e.g.,*[17,21,24–27]).

Because ROS are thought to have been present on Earth for billions of years and to have accompanied the evolution of unicellular and multicellular organisms[28–32], we hypothesized that ROS, and perhaps a ROS-driven cell-to-cell signaling mechanism, like the ROS wave, could have evolved early during the evolution of life on Earth. To test this hypothesis, we studied whether ROS, and in particular an active auto-propagating process of cell-to-cell signaling mediated by ROS (like the ROS wave in flowering plants), can be found in plant lineages that diverged early in the plant phylogeny, including gymnosperms, ferns, lycophytes, bryophytes, multi and unicellular algae, as well as across the animal lineages in amoeba and mammalian cells. Here we show that a ROS-mediated cell-to-cell signaling process can be found in many of these organisms and cells, suggesting that ROS are evolutionarily conserved cell-to-cell signals.

Results

ROS as rapid systemic signals in vascular plants

We previously identified and studied the ROS wave in several different angiosperm species including Arabidopsis, rice, tomato, maize, dandelion, and wheat[20,22,24,33]. However, whether ROS can function as a rapid systemic signal in gymnosperms, as well as other plant lineages is unknown. Here we show that a rapid systemic ROS signal can be triggered by a local treatment of high light (HL) stress in *Pinus sylvestris* (Pine, a Gymnosperm), *Azolla filiculoides* (Azolla, a fern), and *Selaginella moellendorffii* (Selaginella, a Lycopodiaceae; Figure 1). The average rate of the ROS signal measured in these organisms is 0.14 cm min^{-1} (Table S1), faster than the diffusion rate of H_2O_2 in water or biological systems (the diffusion coefficient of H_2O_2 in water or tissues is in the range of 1-2.5 10^{-5} cm^2 min^{-1})[34–36], supporting the active nature of this systemic ROS signal. The findings presented in Figure 1 suggest that rapid systemic ROS signaling is conserved across several different members of the vascular plant family and may have evolved before these lineages diverged from a common ancestor.

Rapid systemic ROS signaling in non-vascular plants

Although the ROS wave was shown to primarily propagate through the vascular bundles of Arabidopsis in response to a local HL stress treatment[37], in response to a local wounding or heat stress treatments it could

also propagate through non-vascular tissues (*i.e.,* mesophyll cells)[38]. We therefore extended our study to include Bryophytes (hornworts, liverworts, and mosses) that emerged from an early split in the diversification of land plants and lack lignified vascular tissues[39]. As shown in Figure 2, a localized treatment of HL caused the activation of a rapid systemic ROS signal in *Anthoceros agrestis* (a Hornwort), *Marchantia polymorpha* (a Liverwort), and *Physcomitrium patens* (Physcomitrella, a Moss), with an average velocity of 0.13 cm min^{-1} (Table S1). These findings suggest that rapid systemic ROS signals are conserved across all land plants and can spread in a systemic manner within or between plants, even in plants that lack a true vascular tissue.

Rapid systemic ROS signaling in multicellular algae and unicellular organisms

The findings that rapid systemic ROS signals are conserved among many land plants (Figures 1 and 2)[20,22,24,33] prompted us to test whether they can also be found in multicellular (*Chara vulgaris*) and unicellular (*Chlamydomonas reinhardtii*) algae. Multicellular and unicellular algae are known to use extracellular ROS as signals and contain NOX/RBOH enzymes[40,41]. As shown in Figures 3a and 3b, a localized treatment of HL stress caused the activation of a rapid systemic ROS response in *Chara vulgaris* grown in liquid medium (velocity of 0.14 cm min^{-1}; Table S1), as well as in *Chlamydomonas reinhardtii* grown as a lawn on an agar plate (velocity of 0.12 cm min^{-1}; Table S1). These findings suggest that ROS can be used as rapid systemic signals even by unicellular organisms and may have evolved as a cell-to-cell signaling mechanism before multicellularity emerged.

The findings that rapid systemic ROS signaling can be found in unicellular alga (Figure 3b) prompted us to test whether it can also be found in other unicellular organisms, such as the soil dwelling amoeba *Dictyostelium discoideum*, that contains NOX and uses extracellular ROS for signaling[41–43]. As shown in Figure 3c, a localized treatment of heat injury caused the activation of a rapid systemic ROS signal in the amoeba *Dictyostelium discoideum* grown on agar plates (velocity of 0.2 cm min^{-1}; Table S1).

Initiation and inhibition of the ROS wave in *Physcomitrella, Chlamydomonas*, and *Dictyostelium*

Two important characteristics of the ROS wave are that it can be triggered by a localized application of H_2O_2 and that once activated it can be blocked by the application of diphenyleneiodonium chloride (DPI; a broad-spectrum NOX/RBOH inhibitor) at a distant location away from its initiation site[19–21]. As shown in Figure 4, application of a 1 µl drop of 10 mM H_2O_2 to *Physcomitrella, Chlamydomonas*, or *Dictyostelium*, grown on agar plates, triggered a rapid systemic ROS signal. In contrast, application of mock buffer to cells,

125 or application of 1 µl drop of 10 mM H_2O_2 to agar plates that contain no cells, did not result in a ROS signal.
126 To further test for H_2O_2 diffusion on plates that had no cells grown on them (live cells are required for
127 H_2DCFDA to generate a signal)[44], we used 2',7'-dichlorodihydrofluorescein (DCF; OxyBurst; 50 µM)[19] to
128 image H_2O_2 in empty plates following the application of 1 µl of 10 mM, or 1 M H_2O_2. As shown in Figure
129 S1, we could not detect the 1 µl of 10 mM H_2O_2, a concentration that resulted in a detectable ROS signal
130 in plates with the different organisms (Figure 4) but were able to detect the 1 µl of 1 M H_2O_2. This finding
131 suggests that the living cells of the different organisms shown in Figure 4 amplified the 1 µl of 1 mM H_2O_2
132 to detectable levels.

133 To test the effect of the RBOH/NOX inhibitor DPI on the propagation of the rapid systemic ROS signal in
134 *Physcomitrella, Chlamydomonas*, or *Dictyostelium*, grown on agar plates, we applied water or DPI (50 µM)
135 in a 1 mm wide strip of agar to the middle of plates, waited 5 min and applied HL or heat injury at one end
136 of the plate (Figure 5a). As shown in Figure 5b, application of DPI (but not water) to the middle of the plate
137 blocked the progression of the cell-to-cell ROS signal. The findings presented in Figures 4 and 5 suggest
138 that the rapid systemic ROS signal, observed as propagating from the initial site of HL or heat injury on
139 plates in the different organisms shown in Figures 2-4, is auto-propagating and resembles the ROS wave
140 discovered and studied in *Arabidopsis thaliana*[19–21,37,38].

141

142 **Functional analysis of the rapid cell-to-cell systemic ROS signal in *Chlamydomonas reinhardtii***

143 To test whether the systemic ROS signal observed in the unicellular alga *Chlamydomonas reinhardtii*
144 (Figures 3-5) can transfer a biologically relevant signal between different cells that are at two ends of the
145 signal path (*i.e.,* local and systemic, on two ends of the agar plate; Figure 6a), we applied HL stress to one
146 corner of a lawn of *Chlamydomonas* cells and sampled these cells, as well as cells that are on the other end
147 of the plate (*i.e.,* not subjected to the HL stress treatment; Figure 6a). We then tested the expression of a
148 HL-response small heat shock protein (sHSP17.1) in cells located at the two ends of the signal path
149 following the application of HL stress to one end of the plate (stressed cells; local). As shown in Figure 6b,
150 the expression of sHSP17.1 was elevated at both ends of the signal path (local and systemic; Figure 6a)
151 suggesting that the ROS wave signal connecting these cells is conveying a stress response signal from the
152 stressed cells (local) to the non-stressed cells (systemic) that did not sense the stress.

153 To test whether inhibiting the ROS wave in *Chlamydomonas* growing on an agar plate (Figure 5) would
154 inhibit the transfer of the stress-response signal from one side of the plate to the other (Figure 6b), we
155 applied DPI (50 µM) or water at the middle point between the stressed cells and the cells that did not sense
156 the stress (similar to Figure 5; Figure 6a). As shown in Figure 6c, DPI, but not water, inhibited the

157 expression of sHSP17.1 in the non-stressed (systemic) cells following the application of HL stress to the
158 stressed cells (local) that are on the other end of the plate. In contrast, DPI or water did not inhibit the
159 expression of sHSP17.1 at the stressed cells (local). These findings suggest that the cell-to-cell ROS signal
160 connecting the two ends of the *Chlamydomonas* lawn growing on the agar plate transfers biologically
161 relevant signals between cells.

162

163 **Cell-to-cell ROS signaling in mammalian cells**

164 The findings that the ROS wave could be found in the amoeba *Dictyostelium discoideum* (Figure 3c),
165 demonstrated that organisms that are outside the plant and algal lineages could use ROS as a cell-to-cell
166 signaling mechanism. *Dictyostelium discoideum* was previously found to contain an ancestral form of
167 NOX[28,41,43], suggesting that other organisms that contain NOX enzymes (for example mammalian cells)
168 could be using ROS for rapid cell-to-cell signaling. To test this possibility, we studied cell-to-cell ROS
169 signaling in monolayers of human (*Homo sapiens*) epithelial breast cancer (MDA-MB-231), and rat (*Rattus*
170 *norvegicus*) cardiomyocytes (H9c2), cells grown in culture. As shown in Figure 7a, wounding of a
171 monolayer of MDA-MB-231 or H9c2 cells with a heated rod resulted in a ROS signal that spread from the
172 injury site at a velocity of 0.28 or 0.2 cm min^{-1} (Table S1), respectively. In the case of H9c2 cells, the ROS
173 signal appeared to travel away from the wound site and to do so in a directional manner, suggesting that the
174 ROS signal observed is not simply ROS that are diffusing away from the initial wound site in all directions
175 (Figure 7a; Movie S1). To determine that the spreading ROS signal was not a result of cell migration and/or
176 monolayer detachment, we conducted microscopic analysis of H9c2 cells at the end the ROS imaging
177 experiments. This analysis revealed that the wound site had an average diameter of 300-600 μm and that
178 cells did not detach or migrate away from it (Figure S2). Moreover, migration of cells away from the wound
179 site would have been much slower (1–10 μm min^{-1})[45] than the rate of the signal observed (0.2 cm min^{-1};
180 Table S1). In addition, to test that H_2O_2 can be detected in all H9c2 cells on the plates (not only the cells
181 observed generating ROS after wounding; Figure 7a), we treated the entire plate with a final concentration
182 of 1 mM H_2O_2 at the end of the experiment (Figure S3). This analysis revealed that all cells on the plate
183 were able to uptake the H_2DCFDA dye, and that H_2O_2 that was provided to the media and entered cells
184 generated a signal [for H_2DCFDA to generate a fluorescent signal at the rapid rate the signal is developing
185 (Figure 7a), it has to enter live cells][44]. To test whether the ROS signal observed in MDA-MB-231 or H9c2
186 is associated with NOX function, we applied DPI (50 μM) or buffer (mock) to these cells prior to the heat
187 injury. As shown in Figure 7b, DPI, but not buffer, caused the complete suppression of the ROS signal.

188

189 **Cell-to-cell ROS signaling in isolated mice hearts**

190 The finding of a ROS wave-like signaling process in rat cardiomyocytes grown in culture (Figure 7)
191 prompted us to test whether a similar process could be found in isolated hearts obtained from mice. For this
192 purpose, we collected hearts from 9-10-weeks-old female and male C57BL/6J mice and incubated them
193 with H_2DCFDA for 2 hours. We then wounded the isolated hearts using an open-flamed-heated rod and
194 imaged ROS responses in the entire isolated heart. As shown in Figures 8a, S4, and Movie S2, wounding
195 of isolated hearts from female or male mice resulted in a ROS response that originated from the point of
196 wounding and progressed at an average rate of 0.106 cm min^{-1} (Table S1) to other parts of the heart. As
197 shown in Figures 8b and S4, this process was inhibited by DPI application to hearts 30 min prior to
198 wounding. These findings suggest that a ROS wave-like signaling process could occur in isolated heart
199 tissue.

200

201

202 **Discussion**

203 The steady-state level of ROS in cells can vary in response to different environmental conditions, the
204 activation of developmental programs that cause active production of ROS, and/or a decline in the activity
205 of ROS scavenging mechanisms[46–48]. ROS can also diffuse into or out of cells through aquaporins, further
206 impacting intracellular ROS levels[47,48]. Because ROS affect the redox state of cells and can alter gene
207 expression through oxidative post-translational modifications (oxi-PTMs) of different proteins[47], they
208 function as key signal transduction molecules involved in the sensing of stress and/or the activation of
209 different developmental programs[48].

210 Because ROS can be transported in or out of cells through aquaporins and/or other channels/pores, secretion
211 of ROS by one cell can alter the redox state of a neighboring cell, thereby altering gene expression within
212 it. This type of paracrine signaling is thought to play an important role in cell-to-cell signaling occurring in
213 different communities of microorganisms, during algal blooms, during interactions between neurons, or
214 during the recruitment of leukocytes to wound sites[49–53]. A central feature of this paracrine signaling
215 mechanisms is however that it may depend on a gradient of ROS forming from the secreting cell(s) to the
216 accepting cell(s). In addition, ROS can be scavenged in route from one cell to the other, limiting the range
217 of this signaling pathway. Having the ability to amplify and maintain cell-to-cell ROS signals, like the auto-
218 propagating ROS wave process in plants[19–21,37,38], would improve the communication between cells in a
219 biofilm/community/tissue and allow them to respond faster and in unison (Figure 9). Here we demonstrate

220 that *Physcomitrella, Chlamydomonas*, and *Dictyostelium*, growing on agar plates, and mammalian cells
221 growing in culture, indeed have the capacity to amplify and maintain cell-to-cell ROS signals (Figures 3-
222 7; Table S1). We further show that cell-to-cell ROS signaling may also occur in isolated mice hearts (Figure
223 8). These findings suggest that the ROS wave signaling process, that was originally discovered in flowering
224 plants[19–21,37,38], could have originated early in evolution and is conserved between plants, microorganisms,
225 and animals. In support of these data are the findings that the systemic ROS signal could be initiated by
226 H_2O_2 (Figure 4), and that application of DPI at a location that is away from the initiation site could block it
227 (Figure 5). Moreover, in H9c2 cells, the peak of the ROS signal propagated in a directional manner at a rate
228 of 0.2 cm min^{-1} departing from its original initiation site and continuing to move away from it in a manner
229 that clearly suggests it is not mediated by simple diffusion (Figures 7 and S3; Movie S1). Although the
230 directionality of the ROS signal (Figures 7 and S3; Movie S1) could be related to cell polarity, it is unknown
231 at present what is the mechanism that govern it. A similar directional spread of the ROS signal was also
232 observed in isolated hearts (Figure 8; Movie S2), further supporting the notion that it is not a simple
233 diffusion process. In addition, the rate of the ROS signal observed in hearts was also faster than that of
234 H_2O_2 in biological systems or water (Table S1)[34–36]. Taken together, these findings suggest that the ROS
235 signal observed in a monolayer of H9c2 cells (Figure 7), or isolated hearts (Figure 8), is driven by an active
236 process of ROS production (that could be inhibited by DPI; Figures 7 and 8), involving multiple cells along
237 its path (*i.e.,* not only cells at and around the injury site).

238 An interesting analogy to the cell-to-cell ROS wave signaling process of plants is the synchronized process
239 of mitochondrial ROS flushes that occurs in mitochondria that are arranged in a lattice formation in muscle
240 tissue (*e.g.,* [54,55]). In this process the release of ROS through pores from one mitochondrion results in the
241 release of ROS from a neighboring mitochondrion spreading from mitochondria-to-mitochondria in a ROS-
242 induced-ROS-release fashion[54,55]. In the context of our findings, that a similar process of cell-to-cell ROS
243 signaling occurs in many different unicellular and multicellular organisms (Figures 1-8), it is possible that
244 even ancient prokaryotic organisms that were the progenitors of mitochondria used this type of cell-to-cell
245 signaling to orchestrate responses within a biofilm or a colony. It is also possible that mitochondria are
246 actively involved in the cell-to-cell ROS signal found in H9c2 cells or hearts (Figures 7 and 8), and that
247 NOXs such as NOX4 that is associated with mitochondria in mammalian cells[56] are mediating this process.
248 Further studies are needed to address the potential role of mitochondria in cell-to-cell ROS signaling.

249 In addition to paracrine signaling, cells can use juxtacrine signaling to exchange ROS with each other[57]. To
250 use this route, however, the levels of ROS transported cannot be too high, as the transmitting or receiving
251 cells could be damaged. Cells living within a biofilm, colony, and/or within different plant and animal
252 tissues, are thought to use juxtacrine signalling to mediate cell-to-cell ROS and redox signaling[10,11].

253 Moreover, it was suggested that ROS can enhance the size of tunneling nanotubes or PDs and facilitate
254 juxtacrine signalling[23,57]. Because we did not distinguish between paracrine and juxtacrine signalling in our
255 study, we cannot rule out the possibility that the cells we imaged used one or the other, or both, for the
256 process of cell-to-cell ROS signaling. In this respect it should be mentioned that our studies of the ROS
257 wave in plants have shown that for cell-to-cell paracrine ROS signaling to occur, juxtacrine signalling must
258 also occur, as key proteins localized to the PD must be present[23]. Paracrine and juxtacrine signalling might
259 therefore be linked in other organisms and this aspect of cell-to-cell ROS signaling should be addressed in
260 future studies.

261 Cancer cells use ROS to regulate their own proliferation and to communicate with cancer-associated
262 macrophages and other host cells (*e.g.,* [58]). In addition, ROS plays a key role in cancer metastasis (*e.g.,* [59]).
263 Our findings that cancer cells can generate and transmit long distance ROS signals (Figure 7), could suggest
264 that a similar process may occur within the tumor microenvironment. This finding should be further studied
265 as it may affect the development of new cancer fighting drugs. In the heart, ROS were implicated in
266 ischemia reperfusion (IR) injury, both in the acute setting of myocardial infarction (MI), as well as in the
267 chronic remodeling process following a MI (*e.g.,* [60–62]). Our findings that cardiomyocytes can use ROS for
268 cell-to-cell communication (Figure 7; Movie S1), and that an active process of ROS signaling is triggered
269 in isolated hearts upon localized wounding (Figure 8), could suggest that enhanced ROS production during
270 IR could trigger different ROS signals that would augment or suppress the tissue damage caused during IR
271 injury. This finding should also be further studied as it could lead to the development of new therapies that
272 will limit tissue damage during IR.

273 Taken together, our findings suggest that cell-to-cell ROS signaling evolved before unicellular and
274 multicellular organisms diverged (Figures 1-8)[19–24]. Because ROS are thought to have been present on Earth
275 for billions of years and could be used to sense the cell's environment through changes in the redox status
276 of the cell[28,32,47,48], it is possible that a cell-to-cell process that uses ROS as a signal evolved early in
277 evolution. This mechanism could have communicated an environmental stress signal that altered the redox
278 state of one cell (the initiating cell) through ROS secreted or transported by this cell to an acceptor cell
279 (Figure 9). The changes in redox state caused by the perceived ROS signal in the acceptor cell would
280 therefore have 'mirrored' the redox state of the initiating cell and information in the form of a 'redox
281 change' transmitted from one cell to the other (Figure 9). The changes in redox state occurring in each of
282 the two cells could cause ROS accumulation and activate gene expression through oxi-PTMs linking the
283 gene expression and ROS responses of both cells (Figure 9). Since the redox state of other neighboring cells
284 will also be altered in a similar manner during this process (like the redox changes that occur in cells along
285 the path of the ROS wave in plants)[63], and these cells will also start accumulating and secreting ROS, the

entire colony, biofilm, or tissue would respond in unison to the stress perceived by the initiating cell (Figure 9), improving its chances of acclimation to the sensed stress, as well as overall survival. Such a mechanism could have coordinated the redox and ROS accumulation responses of a network of cells and give this cell population a better chance of survival in the early environment that was present on Earth; and may have been conserved in one form or another in different organisms to date (Figures 1-8)[19–24]. ROS such and H_2O_2 could have therefore served as one of the first 'stress hormones' on Earth; and to induce a response, the level of this stress hormone (*i.e.,* H_2O_2) had to be increased (Figures 1-9). Our findings that an inhibitor of NADPH oxidases (DPI) can inhibit this process in different organisms (Figures 5-8), support the active nature of this process[19–21]. In addition, at least in *Chlamydomonas* we show that the cell-to-cell ROS signal is required for the expression of sHSP17.1 in cells that were not directly subjected to the stress (Figure 6), demonstrating that the systemic cell-to-cell ROS signal conveys important biological information between cells. In future studies it would be interesting to dissect this signaling process in different organisms and to determine whether it is dependent on paracrine, juxtacrine, or a combination of both signaling pathways (as in plants[20,21,23]). In addition, the nature of the ROS producing, transporting, and perceiving mechanisms need to be determined in different organisms. In plants these were found to be RBOHD/RBOHF, the aquaporin PIP2;1, and HPCA1, respectively[19–21,23,37].

Methods

Organisms and stress treatments

The following organisms were studied in this research: *Pinus sylvestris* (TreeHelp, Buffalo, NY, USA); *Azolla filiculoides* (Carolina Biological Supply Company, Burlington, NC, USA), *Selaginella moellendorffii* (Putnam Hill nursery, Forest Hill, MD, USA), *Marchantia polymorpha* (Carolina Biological Supply Company, Burlington, NC, USA), *Anthoceros agrestis* (a kind gift from Prof. Fay-Wei Li, Cornell University), *Physcomitrium patens* (a kind gift from Prof. Elisabeth Haswell, Washington University at St. Louis and International Moss Stock Center, and Prof. Ralf Reski, University of Freiburg, Freiburg, Germany), *Chara vulgaris* (Carolina Biological Supply Company, Burlington, NC, USA), *Chlamydomonas reinhardtii* (UTEX Culture Collection of Algae, Austin, TX, USA), *Dictyostelium discoideum* (a kind gift from Prof. Thierry Soldati, University of Geneva, and Carolina Biological Supply Company, Burlington, NC, USA), and H9c2 and MDA-MB-231 (ATCC, Manassas, VA, USA). Organisms were grown according to stock resource instructions. Photosynthetic organisms were grown under 8 hrs/ 16 hrs light/dark regime. *P. sylvestris, S. moellendorffii and M. polymorpha* were grown in peat pellets (Jiffy-7, Jiffy International,

318 Kristiansand, Norway)[20,21]. *A. filiculoides* was grown in 0.25 MS liquid media[64]; *A. agrestis* was grown on
319 a solid modified Hatcher medium[65]; *P. patens* was grown on BCD solid media[66]; *Chara vulgaris* was grown
320 in a Broyer and Barr liquid media[67]; *C. reinhardtii* cultures were grown on P49 solid media (UTEX Culture
321 Collection of Algae, Austin, TX, USA); *D. discoideum* cultures were grown on SM agar plates in room
322 temperature[68]. Mammalian cells were grown in 37°C 5% CO_2 RPMI medium 1640 supplemented with 10%
323 FCS, L- glutamine, and antibiotics (ThermoFisher, Waltham, MA)[69]. A day before the experiment the
324 media was replaced with FluoroBrite DMEM (ThermoFisher, Waltham, MA) to reduce background
325 fluorescence[70]. For organisms treated with local HL stress, following fumigation with H_2DCFDA solution,
326 illumination of 1700 µmol photons m^{-2} s^{-1} was applied to a local leaf/area for 2 min using a fiber optic
327 (Schott, Southbridge, MA, USA), as described previously[20,23,27,37]. Heat injury, following treatment of
328 H_2DCFDA was applied for *D. discoideum* and mammalian cells using an open-flame-heated metal rod[22]
329 that touched the local injury area for 1 second[22]. Hydrogen peroxide was applied as a 1 µl drop of 10 mM
330 diluted in the buffer of the medium in which the organism was cultured. Diphenyleneiodonium chloride
331 (DPI; 50 µM) or water were applied as a strip of 0.05% agarose (applied with a pipette tip along the center
332 of the plate; Figure 5A) for *P. patens*, *C. reinhardtii* and *D. discoideum*, or in the media for mammalian
333 cells 5 or 10 min prior to the stress application[20].

334 **Isolated heart studies**

335 Mice used in this study were housed under pathogen-free conditions in animal care facilities and received
336 humane care in compliance with the Guide for the Care and Use of Laboratory Animals
337 (https://www.ncbi.nlm.nih.gov/books/NBK54050/)[71]. All experimental procedures were approved by the
338 Institutional Animal Care and Use Committee of the University of Missouri
339 (https://research.missouri.edu/acqa/acuc). C57BL/6J mice were obtained from Jackson Laboratory
340 (https://www.jax.org/) at 8 weeks of age and used between the age of 9 and 10 weeks of age. Mice were
341 placed under anesthesia using 4% Isoflurane, sacrificed, and the hearts were immediately collected[71]. The
342 hearts were rinsed in FluoroBrite DMEM (ThermoFisher, Waltham, MA) to remove excess blood. They
343 were then incubated in Fluro Bright DMEM media containing 10% Fetal Bovine Serum, 15 mM Hepes, 50
344 µM H_2DCFDA (Millipore-Sigma, St. Louis, MO, USA), and Penicillin-Streptomycin 10,000 Units/ml
345 (Gibco; ThermoFisher, Waltham, MA) for 2 hrs with gentle rocking in a CO_2 incubator (Binder C170;
346 ThermoFisher, Waltham, MA). For DPI treatments, DPI (50 µM final concentration) was added to the
347 incubation media 30 min prior to imaging. Isolated hearts were then wounded or unwounded with an open-
348 flame-heated rod[22] and immediately imaged as described below.

349

350 **ROS imaging**

351 All organisms, outside of mammalian cells and isolated hearts, were fumigated with 50 μM H_2DCFDA
352 (Millipore-Sigma, St. Louis, MO, USA) in 0.05 M Phosphate buffer pH 7.4 with 0.01% Silwet L-77.
353 Fumigation was carried out for 30 min using nebulizers (Punasi Direct, Hong Kong, China)[20–24,37,38]. For
354 mammalian cells and isolated hearts 10 μM H_2DCFDA (final concentration) was applied to the medium for
355 30 min (cell cultures), or 2 hrs (isolated hearts). Following H_2DCFDA fumigation/incubation, local
356 stress/wounding was applied, and organisms/isolated hearts were imaged for live ROS accumulation using
357 the IVIS Lumina S5 platform[20–24,37,38,72]. Acquired images were then analyzed using the math function in
358 Living Image software (PerkinElmer, Waltham, MA, USA) [20–24,37,38]. Empty agar plates were also fumigated
359 with 2',7'-dichlorodihydrofluorescein (DCF; OxyBurst; 50 μM)[19], treated with H_2O_2 and imaged as
360 described above.

361 **Protein blot analysis**

362 Local and systemic cells of *C. reinhardtii* from treated or untreated plates, with or without DPI, 2 min or
363 30 min after a 2 min HL treatment were collected and denatured by boiling in 4 x Laemmli buffer. The
364 samples were spun down and the supernatant was loaded on SDS-PAGE and blotted to PVDF membrane.
365 Polyclonal anti-sHSP17.1 antibodies from rabbit were used to identify the proteins on the membrane as
366 described previously[24,25].

367 **Statistical analysis**

368 All experiments were repeated at least three times with at least 3 biological repeats. Box plots graphs are
369 presented with mean as X ± SE; median is line in the box and box borders are 25th and 75th percentiles;
370 whiskers are the 1.5 interquartile range. Paired Student t-test was conducted using Microsoft Excel (*P <
371 0.05; **P < 0.01; ***P < 0.001).

372 **Acknowledgements**

373 We thank Professor Brent Mishler for discussions regarding which organisms to target for our evolutionary
374 analysis. We also thank Professor Thierry Soldati for gift of *Dictyostelium discoideum*, Professor Elisabeth
375 Haswell and Professor Ralf Reski for gift of *Physcomitrium patens*, and Professor Fay-Wei Li for gift of
376 *Anthoceros agrestis*.

377 **Funding**

378 This work was supported by funding from the National Science Foundation grants IOS-1932639, National
379 Institute of Health GM111364, and the Interdisciplinary Plant Group, University of Missouri.

380 **References**

381 1. Miller, M.B., and Bassler, B.L. (2001). Quorum sensing in bacteria. Annu. Rev. Microbiol. *55*, 165–
382 199.

383 2. Fan, Q., Wang, H., Mao, C., Li, J., Zhang, X., Grenier, D., Yi, L., and Wang, Y. (2022). Structure and
384 signal regulation mechanism of interspecies and interkingdom quorum sensing system receptors. J.
385 Agric. Food Chem. *70*, 429–445.

386 3. Gambino, M., and Cappitelli, F. (2016). Mini-review: Biofilm responses to oxidative stress. Biofouling
387 *32*, 167–178.

388 4. Mahto, K.U., Kumari, S., and Das, S. (2022). Unraveling the complex regulatory networks in biofilm
389 formation in bacteria and relevance of biofilms in environmental remediation. Crit. Rev. Biochem.
390 Mol. Biol. *57*, 305–332.

391 5. Holland, N.D. (2003). Early central nervous system evolution: an era of skin brains? Nat. Rev.
392 Neurosci. *4*, 617–627.

393 6. Ovsepian, S.V., O'Leary, V.B., and Vesselkin, N.P. (2020). Evolutionary origins of chemical synapses.
394 Vitam. Horm. *114*, 1–21.

395 7. Chávez, A.S.O., O'Neal, A.J., Santambrogio, L., Kotsyfakis, M., and Pedra, J.H.F. (2019). Message in
396 a vesicle - trans-kingdom intercommunication at the vector-host interface. J. Cell Sci. *132*, jcs224212.

397 8. Zhou, Q., Ma, K., Hu, H., Xing, X., Huang, X., and Gao, H. (2022). Extracellular vesicles: Their
398 functions in plant–pathogen interactions. Mol. Plant Pathol. *23*, 760–771.

399 9. Marchionni, M.A. (2014). Neuregulin signaling in pieces-evolution of the gene family. Curr. Pharm.
400 Des. *20*, 4856–4873.

401 10. Matkó, J., and Tóth, E.A. (2021). Membrane nanotubes are ancient machinery for cell-to-cell
402 communication and transport. Their interference with the immune system. Biol. Futura *72*, 25–36.

403 11. Ariazi, J., Benowitz, A., De Biasi, V., Den Boer, M.L., Cherqui, S., Cui, H., Douillet, N., Eugenin,
404 E.A., Favre, D., Goodman, S., et al. (2017). Tunneling Nanotubes and Gap junctions-their role in long-
405 range intercellular communication during development, health, and disease conditions. Front. Mol.
406 Neurosci. *10*, 333.

407 12. Combarnous, Y., and Nguyen, T.M.D. (2020). Cell communications among microorganisms, plants,
408 and animals: Origin, evolution, and interplays. Int. J. Mol. Sci. *21*, E8052.

409 13. Ghanam, J., Chetty, V.K., Barthel, L., Reinhardt, D., Hoyer, P.-F., and Thakur, B.K. (2022). DNA in
410 extracellular vesicles: from evolution to its current application in health and disease. Cell Biosci. *12*,
411 37.

412 14. Anfang, M., and Shani, E. (2021). Transport mechanisms of plant hormones. Curr. Opin. Plant Biol.
413 *63*, 102055.

414 15. Furumizu, C., Krabberød, A.K., Hammerstad, M., Alling, R.M., Wildhagen, M., Sawa, S., and Aalen,
415 R.B. (2021). The sequenced genomes of nonflowering land plants reveal the innovative evolutionary
416 history of peptide signaling. Plant Cell *33*, 2915–2934.

417 16. Farmer, E.E., Gao, Y.-Q., Lenzoni, G., Wolfender, J.-L., and Wu, Q. (2020). Wound and
418 mechanostimulated electrical signals control hormone responses. New Phytol. *227*, 1037–1050.

419 17. Fichman, Y., and Mittler, R. (2021). Integration of electric, calcium, reactive oxygen species and
420 hydraulic signals during rapid systemic signaling in plants. Plant J. *107*, 7–20.

421 18. Shao, Q., Gao, Q., Lhamo, D., Zhang, H., and Luan, S. (2020). Two glutamate- and pH-regulated Ca2+
422 channels are required for systemic wound signaling in Arabidopsis. Sci. Signal. *13*, aba1453.

423 19. Miller, G., Schlauch, K., Tam, R., Cortes, D., Torres, M.A., Shulaev, V., Dangl, J.L., and Mittler, R.
424 (2009). The plant NADPH oxidase RBOHD mediates rapid systemic signaling in response to diverse
425 stimuli. Sci. Signal. *2*, ra45–ra45.

426 20. Fichman, Y., Miller, G., and Mittler, R. (2019). Whole-plant live imaging of reactive oxygen species.
427 Mol. Plant *12*, 1203–1210.

428 21. Fichman, Y., Zandalinas, S.I., Peck, S.C., Luan, S., and Mittler, R. (2022). HPCA1 is required for
429 systemic ROS and calcium cell-to-cell signaling and plant acclimation to stress. Plant Cell,
430 10.1093/plcell/koac241.

431 22. Szechynska-Hebda, M., Lewandowska, M., Witoń, D., Fichman, Y., Mittler, R., and Karpinski, S.
432 (2022). Aboveground plant-to-plant electrical signaling mediates network acquired acclimation. Plant
433 Cell *34*, 3047–3065.

434 23. Fichman, Y., Myers, R.J., Grant, D.G., and Mittler, R. (2021). Plasmodesmata-localized proteins and
435 ROS orchestrate light-induced rapid systemic signaling in Arabidopsis. Sci. Signal. *14*, eabf0322.

436 24. Fichman, Y., Xiong, H., Sengupta, S., Azad, R.K., Hibberd, J.M., Liscum, E., and Mittler, R. (2021).
437 Phytochrome B regulates reactive oxygen signaling during abiotic and biotic stress in plants. BioRxiv,
438 2021.11.29.470478.

439 25. Suzuki, N., Miller, G., Salazar, C., Mondal, H.A., Shulaev, E., Cortes, D.F., Shuman, J.L., Luo, X.,
440 Shah, J., Schlauch, K., et al. (2013). Temporal-spatial interaction between reactive oxygen species and
441 abscisic acid regulates rapid systemic acclimation in plants. Plant Cell *25*, 3553–3569.

442 26. Zandalinas, S.I., Sengupta, S., Burks, D., Azad, R.K., and Mittler, R. (2019). Identification and
443 characterization of a core set of ROS wave-associated transcripts involved in the systemic acquired
444 acclimation response of Arabidopsis to excess light. Plant J. *98*, 126–141.

445 27. Zandalinas, S.I., Fichman, Y., Devireddy, A.R., Sengupta, S., Azad, R.K., and Mittler, R. (2020).
446 Systemic signaling during abiotic stress combination in plants. Proc. Natl. Acad. Sci. U.S.A. *117*,
447 13810–13820.

448 28. Inupakutika, M.A., Sengupta, S., Devireddy, A.R., Azad, R.K., and Mittler, R. (2016). The evolution
449 of reactive oxygen species metabolism. J. Exp. Bot. *67*, 5933–5943.

450 29. Taverne, Y.J., Merkus, D., Bogers, A.J., Halliwell, B., Duncker, D.J., and Lyons, T.W. (2018).
451 Reactive oxygen species: Radical factors in the evolution of animal life. BioEssays *40*, 1700158.

452 30. Hörandl, E., and Speijer, D. (2018). How oxygen gave rise to eukaryotic sex. Proc. Royal Soc. B *285*,
453 20172706.

454 31. Gutteridge, J.M.C., and Halliwell, B. (2018). Mini-Review: Oxidative stress, redox stress or redox
455 success? Biochem. Biophys. Res. Commun. *502*, 183–186.

456 32. Jabłońska, J., and Tawfik, D.S. (2021). The evolution of oxygen-utilizing enzymes suggests early
457 biosphere oxygenation. Nat. Ecol. Evol. *5*, 442–448.

458 33. Fichman, Y., and Mittler, R. (2020). Noninvasive live ROS imaging of whole plants grown in soil.
459 Trends Plant Sci. *25*, 1052–1053.

460 34. Liu, Z.C., Liu, D.X., Chen, C., Li, D., Yang, A.J., Rong, M.Z., Chen, H.L., and Kong, M.G. (2015).
461 Physicochemical processes in the indirect interaction between surface air plasma and deionized water.
462 J. Phys. D: Appl. Phys. *48*, 495201.

463 35. Ledo, A., Fernandes, E., Salvador, A., Laranjinha, J., and Barbosa, R.M. (2022). In vivo hydrogen
464 peroxide diffusivity in brain tissue supports volume signaling activity. Redox Biol. *50*, 102250.

465 36. Tjell, A.Ø., and Almdal, K. (2018). Diffusion rate of hydrogen peroxide through water-swelled
466 polyurethane membranes. Sens. Bio-Sens. Res. *21*, 35–39.

467 37. Zandalinas, S.I., Fichman, Y., and Mittler, R. (2020). Vascular bundles mediate systemic reactive
468 oxygen signaling during light stress. Plant Cell *32*, 3425–3435.

469 38. Zandalinas, S.I., and Mittler, R. (2021). Vascular and nonvascular transmission of systemic reactive
470 oxygen signals during wounding and heat stress. Plant Physiol. *186*, 1721–1733.

471 39. Fürst-Jansen, J.M.R., de Vries, S., and de Vries, J. (2020). Evo-physio: on stress responses and the
472 earliest land plants. J. Exp. Bot. *71*, 3254–3269.

473 40. Hansel, C.M., and Diaz, J.M. (2021). Production of extracellular reactive oxygen species by marine
474 biota. Ann. Rev. Mar. Sci. *13*, 177–200.

475 41. Kawahara, T., Quinn, M.T., and Lambeth, J.D. (2007). Molecular evolution of the reactive oxygen-
476 generating NADPH oxidase (Nox/Duox) family of enzymes. BMC Evol. Biol. *7*, 109.

477 42. Lardy, B., Bof, M., Aubry, L., Paclet, M.H., Morel, F., Satre, M., and Klein, G. (2005). NADPH
478 oxidase homologs are required for normal cell differentiation and morphogenesis in Dictyostelium
479 discoideum. Biochim. Biophys. Acta *1744*, 199–212.

480 43. Aguirre, J., and Lambeth, J.D. (2010). Nox enzymes from fungus to fly to fish and what they tell us
481 about Nox function in mammals. Free Radic. Biol. Med. *49*, 1342–1353.

482 44. Ortega-Villasante, C., Burén, S., Barón-Sola, Á., Martínez, F., and Hernández, L.E. (2016). In vivo
483 ROS and redox potential fluorescent detection in plants: Present approaches and future perspectives.
484 Methods *109*, 92–104.

485 45. Lauffenburger, D.A., and Horwitz, A.F. (1996). Cell migration: a physically integrated molecular
486 process. Cell *84*, 359–369.

487 46. Smirnoff, N., and Arnaud, D. (2019). Hydrogen peroxide metabolism and functions in plants. New
488 Phytol. *221*, 1197–1214.

489 47. Sies, H., and Jones, D.P. (2020). Reactive oxygen species (ROS) as pleiotropic physiological signalling
490 agents. Nat. Rev. Mol. Cell Biol. *21*, 363–383.

491 48. Mittler, R., Zandalinas, S.I., Fichman, Y., and Van Breusegem, F. (2022). Reactive oxygen species
492 signalling in plant stress responses. Nat. Rev. Mol. Cell Biol., 10.1038/s41580-022-00499–2.

493 49. Čáp, M., Váchová, L., and Palková, Z. (2012). Reactive Oxygen Species in the signaling and adaptation
494 of multicellular microbial communities. Oxid. Med. Cell. Longev. *2012*, e976753.

495 50. Zheng, H., Kim, J., Liew, M., Yan, J.K., Herrera, O., Bok, J.W., Kelleher, N.L., Keller, N.P., and
496 Wang, Y. (2015). Redox metabolites signal Polymicrobial biofilm development via the NapA oxidative
497 stress cascade in Aspergillus. Curr. Biol. *25*, 29–37.

498 51. Sukenik, A., and Kaplan, A. (2021). Cyanobacterial harmful algal blooms in aquatic ecosystems: A
499 comprehensive outlook on current and emerging mitigation and control approaches. Microorganisms
500 *9*, 1472.

501 52. Martínez-Navarro, F.J., Martínez-Morcillo, F.J., de Oliveira, S., Candel, S., Cabas, I., García-Ayala,
502 A., Martínez-Menchón, T., Corbalán-Vélez, R., Mesa-Del-Castillo, P., Cayuela, M.L., et al. (2020).
503 Hydrogen peroxide in neutrophil inflammation: Lesson from the zebrafish. Dev. Comp. Immunol. *105*,
504 103583.

505 53. Iwashita, H., Castillo, E., Messina, M.S., Swanson, R.A., and Chang, C.J. (2021). A tandem activity-
506 based sensing and labeling strategy enables imaging of transcellular hydrogen peroxide signaling. Proc.
507 Natl. Acad. Sci. U.S.A. *118*, e2018513118.

508 54. Kuznetsov, A.V., Javadov, S., Saks, V., Margreiter, R., and Grimm, M. (2017). Synchronism in
509 mitochondrial ROS flashes, membrane depolarization and calcium sparks in human carcinoma cells.
510 Biochim. Biophys. Acta Bioenerg. *1858*, 418–431.

511 55. Chen, W., Luo, S., Xie, P., Hou, T., Yu, T., and Fu, X. (2018). Overexpressed UCP2 regulates
512 mitochondrial flashes and reverses lipopolysaccharide-induced cardiomyocytes injury. Am. J. Transl.
513 Res. *10*, 1347–1356.

514 56. Buvelot, H., Jaquet, V., and Krause, K.-H. (2019). Mammalian NADPH oxidases. In NADPH
515 Oxidases: Methods and Protocols Methods in Molecular Biology., U. G. Knaus and T. L. Leto, eds.
516 (Humana Press), pp. 17–36.

517 57. Liang, D. (2018). A salutary role of reactive oxygen species in intercellular tunnel-mediated
518 communication. Front. Cell. Dev. Biol. *6*, 2.

519 58. Xing, F., Hu, Q., Qin, Y., Xu, J., Zhang, B., Yu, X., and Wang, W. (2022). The relationship of redox
520 with hallmarks of cancer: The importance of homeostasis and context. Front. Oncol. *12*, 862743.

521 59. Liao, Z., Chua, D., and Tan, N.S. (2019). Reactive oxygen species: a volatile driver of field
522 cancerization and metastasis. Mol. Cancer *18*, 65.

523 60. Tsutsui, H., Kinugawa, S., and Matsushima, S. (2011). Oxidative stress and heart failure. Am. J.
524 Physiol. Heart Circ. Physiol. *301*, H2181–H2190.

525 61. Cadenas, S. (2018). ROS and redox signaling in myocardial ischemia-reperfusion injury and
526 cardioprotection. Free Radic. Biol. Med. *117*, 76–89.

527 62. Bugger, H., and Pfeil, K. (2020). Mitochondrial ROS in myocardial ischemia reperfusion and
528 remodeling. Biochim. Biophys. Acta Mol. Basis Dis. *1866*, 165768.

529 63. Fichman, Y., and Mittler, R. (2021). A systemic whole-plant change in redox levels accompanies the
530 rapid systemic response to wounding. Plant Physiol. *186*, 4–8.

531 64. Murashige, T., and Skoog, F. (1962). A revised medium for rapid growth and bio assays with tobacco
532 tissue cultures. Physiol. Plant. *15*, 473–497.

533 65. Gunadi, A., Li, F.-W., and Van Eck, J. (2022). Accelerating gametophytic growth in the model
534 hornwort Anthoceros agrestis. Appl. Plant Sci. *10*, e11460.

535 66. Cove, D.J., Perroud, P.-F., Charron, A.J., McDaniel, S.F., Khandelwal, A., and Quatrano, R.S. (2009).
536 The Moss Physcomitrella patens: A Novel model System for plant development and genomic studies.
537 Cold Spring Harb. Protoc. *2009*, pdb.emo115.

538 67. Hope, A.B., and Walker, N.A. (1975). The Physiology of Giant Algal Cells (Cambridge University
539 Press).

540 68. Froquet, R., Lelong, E., Marchetti, A., and Cosson, P. (2009). Dictyostelium discoideum: a model host
541 to measure bacterial virulence. Nat. Protoc. *4*, 25–30.

542 69. Sohn, Y.-S., Tamir, S., Song, L., Michaeli, D., Matouk, I., Conlan, A.R., Harir, Y., Holt, S.H., Shulaev,
543 V., Paddock, M.L., et al. (2013). NAF-1 and mitoNEET are central to human breast cancer proliferation
544 by maintaining mitochondrial homeostasis and promoting tumor growth. Proc. Natl. Acad. Sci. U.S.A.
545 *110*, 14676–14681.

546 70. Karmi, O., Holt, S.H., Song, L., Tamir, S., Luo, Y., Bai, F., Adenwalla, A., Darash-Yahana, M., Sohn,
547 Y.-S., Jennings, P.A., et al. (2017). Interactions between mitoNEET and NAF-1 in cells. PLoS One *12*,
548 e0175796.

549 71. Karmi, O., Rowland, L., King, S.D., Manrique-Acevedo, C., Cabantchik, I.Z., Nechushtai, R.,
550 Mittler, R. (2022). The [2Fe-2S] protein CISD2 plays a key role in preventing iron accumulation in
551 cardiomyocytes. FEBS Lett. *596,* 747-761.

552 72. Zhu, Q., Hao, H., Xu, H., Fichman, Y., Cui, Y., Yang, C., Wang, M., Mittler, R., Hill, M.A., Cowan,
553 P.J., et al., (2021). Combination of Antioxidant Enzyme Overexpression and N-Acetylcysteine
554 Treatment Enhances the Survival of Bone Marrow Mesenchymal Stromal Cells in Ischemic Limb in
555 Mice With Type 2 Diabetes. J Am Heart Assoc. *10,* e023491.

556

557 **Figure legends**

558 **Figure 1.** ROS as rapid systemic signals in *Pinus sylvestris*, *Azolla filiculoides*, and *Selaginella*
559 *moellendorffii.* **(a)** *Pinus sylvestris* plants were subjected to a high light (HL) stress treatment applied to a
560 single leaf, and ROS accumulation was imaged, using H_2DCFDA, in whole plants (local and systemic
561 tissues, indicated with solid and dashed circles, respectively). Representative time-lapse images of whole
562 plant ROS accumulation in treated and untreated *Pinus sylvestris* plants are shown alongside bar graphs of
563 combined data from all plants used for the analysis at the 0- and 30-min time points (local and systemic).
564 **(b)** Same as a but for *Azolla filiculoides*. **(c)** Same as a, but for *Selaginella moellendorffii*. All experiments
565 were repeated at least 3 times with 10 plants per experiment. Data is presented as box plot graphs; X is
566 mean ± S.E., N=30, *P < 0.05, **P < 0.01, Student t-test. Scale bar, 1 cm. Abbreviations: H_2DCFDA, 2',7'-
567 dichlorodihydrofluorescein diacetate; HL, high light; L, local; ROS, reactive oxygen species; S, systemic;
568 TRE, total radiant efficiency.

569 **Figure 2.** Rapid systemic ROS signaling in non-vascular plants. **(a)** *Anthoceros agrestis* plants were
570 subjected to a high light (HL) stress treatment applied to a single leaf and ROS accumulation was imaged
571 using H_2DCFDA, in whole plants (local and systemic tissues, indicated with solid and dashed circles,
572 respectively). Representative time-lapse images of whole plant ROS accumulation in treated and untreated
573 *Anthoceros agrestis* plants are shown alongside bar graphs of combined data from all plants used for the
574 analysis at the 0- and 30-min time points (local and systemic). **(b)** Same as a but for *Marchantia*
575 *polymorpha*. **(c)** Same as a, but for *Physcomitrium patens*. All experiments were repeated at least 3 times
576 with 10 plants per experiment. Data is presented as box plot graphs; X is mean ± S.E., N=30, *P < 0.05,
577 **P < 0.01, ***P < 0.001, Student t-test. Scale bar, 1 cm. Abbreviations: H_2DCFDA, 2',7'-
578 dichlorodihydrofluorescein diacetate; HL, high light; L, local; ROS, reactive oxygen species; S, systemic;
579 TRE, total radiant efficiency.

580 **Figure 3.** Rapid systemic ROS signaling in multicellular algae and unicellular organisms. **(a)** *Chara*
581 *vulgaris*, a multicellular alga, was subjected to a high light (HL) stress treatment applied to a single branch,
582 and ROS accumulation was imaged, using H_2DCFDA, in several branches of the alga (local and systemic
583 tissues, indicated with solid and dashed circles, respectively). Representative time-lapse images of whole
584 alga ROS accumulation in treated and untreated *Chara vulgaris* are shown alongside bar graphs of
585 combined data from all plants used for the analysis at the 0- and 30-min time points (local and systemic).
586 **(b)** An agar plate containing a lawn of *Chlamydomonas reinhardtii*, a unicellular alga, was treated with a
587 focused beam of HL (local treatment), and ROS accumulation was imaged, using H_2DCFDA, in the entire
588 plate (local and systemic tissues are indicated with solid and dashed circles, respectively). Representative
589 time-lapse images of whole plate ROS accumulation of treated and untreated *Chlamydomonas* lawn are

590 shown alongside bar graphs of combined data from all plants used for the analysis at the 0- and 30-min time
591 points (local and systemic). **(c)** Same as in b, but for an agar plate that contains a lawn of *Dictyostelium*
592 *discoideum* that was treated locally with a heated rod (local). All experiments were repeated at least 3 times
593 with 10 multicellular alga, or agar plates per experiment. Data is presented as box plot graphs; X is mean ±
594 S.E., N=30, *P < 0.05, **P < 0.01, ***P < 0.001, Student t-test. Scale bar, 1 cm. Abbreviations: H_2DCFDA,
595 2',7'-dichlorodihydrofluorescein diacetate; HL, high light; L, local; ROS, reactive oxygen species; S,
596 systemic; TRE, total radiant efficiency.

597 **Figure 4.** Activation of the rapid systemic ROS signal in *Physcomitrium patens*, *Chlamydomonas*
598 *reinhardtii*, and *Dictyostelium discoideum* by a local application of H_2O_2. **(a)** An agar plate without
599 *Physcomitrium patens* (top), and agar plates with a lawn of *Physcomitrium patens* (middle and bottom),
600 were treated with 1 µl of 1 mM H_2O_2 (top and bottom), or 1 µl of media (mock, middle), and ROS
601 accumulation was imaged using H_2DCFDA in the entire plate. Representative time-lapse images of whole
602 plate ROS accumulation are shown alongside bar graphs of combined data from all plates used for the
603 analysis at the 0- and 30-min time points (local and systemic). Local and systemic sampling locations are
604 indicated with solid and dashed circles, respectively. **(b)** Same as a, but for plates with or without a lawn
605 of *Chlamydomonas reinhardtii*. **(c)** Same as in a, but for plates with or without *Dictyostelium discoideum*.
606 All experiments were repeated at least 3 times with 10 agar plates per experiment. Data is presented as box
607 plot graphs; X is mean ± S.E., N=30, *P < 0.05, **P < 0.01, ***P < 0.001, Student t-test. Scale bar, 1 cm.
608 Abbreviations: H_2DCFDA, 2',7'-dichlorodihydrofluorescein diacetate; HL, high light; L, local; ROS,
609 reactive oxygen species; S, systemic; TRE, total radiant efficiency.

610 **Figure 5.** Inhibition of the rapid systemic ROS signal in *Physcomitrium patens*, *Chlamydomonas*
611 *reinhardtii*, and *Dictyostelium discoideum* by DPI. **(a)** A diagram showing the experimental design used.
612 A strip of agar containing water or the NOX/RBOH inhibitor DPI (50 µM) was layered over the middle of
613 agar plates containing a lawn of the different organisms growing on them. Following a 5 min incubation
614 one side of the plate was treated with a focused beam of high light (HL) or touched with a heated rod (local)
615 and ROS accumulation was imaged using H_2DCFDA in the entire plate. Local and systemic locations used
616 for signal quantification are indicated with solid and dashed circles, respectively. **(b)** Representative time-
617 lapse images of whole plate ROS accumulation are shown alongside bar graphs of combined data from all
618 plates used for the analysis at the 0- and 30-min time points (Water or DPI treated *Physcomitrium patens*,
619 *Chlamydomonas reinhardtii*, or *Dictyostelium discoideum*; top, middle, and bottom, respectively; local and
620 systemic). All experiments were repeated at least 3 times with 10 agar plates per experiment. Data is
621 presented as box plot graphs; X is mean ± S.E., N=30, **P < 0.01, ***P < 0.001, Student t-test. Scale bar,
622 1 cm. Abbreviations: DPI, diphenyleneiodonium; H_2DCFDA, 2',7'-dichlorodihydrofluorescein diacetate;

623 HL, high light; L, local; NOX, NADPH oxidase; RBOH, respiratory burst oxidase homolog; ROS, reactive
624 oxygen species; S, systemic; TRE, total radiant efficiency.

625 **Figure 6.** Functional analysis of the cell-to-cell rapid ROS signal in *Chlamydomonas reinhardtii*. **(a)**
626 Diagrams showing the experimental designs used. Left: A lawn of *Chlamydomonas reinhardtii* growing on
627 an agar plate was subjected to a focused beam of high light (HL) stress and the area subjected to the beam
628 (local, L), as well as an area that is on the other end of the plate (systemic, S) were sampled at different
629 times following the application of HL for analysis of the expression of the light stress response small heat
630 shock protein 17.1 (sHSP17.1; This design was used for the experiments shown in B). Right: A strip of
631 agar containing water or the NOX/RBOH inhibitor DPI (50 μM) was layered over the middle of agar plates
632 containing the lawn of *Chlamydomonas reinhardtii* 5 min prior to the application of light stress and
633 sampling (This design was used for the experiments shown in C). Local and systemic sampling locations
634 are indicated with solid and dashed circles, respectively. **(b)** Representative protein blots and Coomassie-
635 stained gels are shown alongside bar graphs of combined data from all blots used for the analysis at the 0-,
636 2-, and 30-min time points, for the expression of sHSP17.1 in the L and S locations, following the light
637 stress treatment. **(c)** Same as in b, but for experiments in which a strip of agar containing water (left) or DPI
638 (right) was layered over the middle of agar plates 5 min prior to the application of HL stress. All experiments
639 were repeated at least 3 times with 10 agar plates per experiment. Data is presented as box plot graphs; X
640 is mean ± S.E., N=30, *P < 0.05, **P < 0.01, ***P < 0.001, Student t-test. Scale bar, 1 cm. Abbreviations:
641 DPI, diphenyleneiodonium; H_2DCFDA, 2',7'-dichlorodihydrofluorescein diacetate; HL, high light; L, local;
642 NOX, NADPH oxidase; RBOH, respiratory burst oxidase homolog; ROS, reactive oxygen species; S,
643 systemic; sHSP, small heat shock protein 17.1.

644 **Figure 7.** Rapid systemic ROS signaling in mammalian cells. **(a)** Monolayers of human epithelial breast
645 cancer (MDA-MB-231; top), and rat cardiomyocytes (H9c2; bottom), cells grown in culture were treated
646 with a heated metal rod to induce injury (average injury diameter is 120 μm) and ROS accumulation was
647 imaged using H_2DCFDA in the entire plate. Representative time-lapse images of whole plate ROS
648 accumulation in treated and untreated plates are shown alongside bar graphs of combined data from all
649 plates used for the analysis at the 0- and 30-min time points (local and systemic). Local and systemic
650 sampling locations are indicated with solid and dashed circles, respectively. **(b)** Same as in a, except that
651 buffer or DPI (50 μM) were added to the growth media of cells 10 min prior to the heat injury. All
652 experiments were repeated at least 3 times with 10 agar plates per experiment. Data is presented as box plot
653 graphs; X is mean ± S.E., N=30, **P < 0.01, ***P < 0.001, Student t-test. Scale bar, 1 cm. Abbreviations:
654 DPI, diphenyleneiodonium; H_2DCFDA, 2',7'-dichlorodihydrofluorescein diacetate; L, local; ROS, reactive
655 oxygen species; S, systemic; TRE, total radiant efficiency.

656 **Figure 8.** Wound-induced rapid systemic ROS signaling in isolated mice hearts. Mice hearts, surgically
657 removed from 9-10-week-old male and female C57BL/6J mice, were untreated, or treated with a heated
658 metal rod (to induce injury), in the presence or absence of DPI (50 μM), and ROS accumulation was imaged
659 using H_2DCFDA in the entire hearts. Representative time-lapse images of whole heart ROS accumulation
660 **(a)** are shown alongside bar graphs of combined data from all hearts used for the analysis at the 0- and 30-
661 min time points **(b)**. Local and systemic sampling locations are indicated with solid and dashed circles,
662 respectively. All experiments were repeated at least 3 times with 3 female and 3 male mice per experiment.
663 Data is presented as box plot graphs; X is mean ± S.E., N=30, **P < 0.01, ***P < 0.001, Student t-test.
664 Scale bar, 1 cm. Female- and male-specific ROS responses are shown in Figure S4. Abbreviations: DPI,
665 diphenyleneiodonium; H_2DCFDA, 2',7'-dichlorodihydrofluorescein diacetate; L, local; ROS, reactive
666 oxygen species; S, systemic; TRE, total radiant efficiency; w/, with.

667 **Figure 9.** A model depicting the principle of the cell-to-cell ROS signaling pathway that is conserved
668 between unicellular and multicellular organisms. An initiating cell that perceives a stress or ROS signal is
669 shown on the left to undergo a change in redox levels that will cause the accumulation of ROS in that cell.
670 This process is shown to cause the activation of a paracrine and juxtacrine ROS-mediated cell-to-cell signal
671 transduction pathway. Each cell along the path of this pathway accumulates ROS maintaining the signal
672 and transmitting it to the next. The resulting changes in redox in all cells involved in this signaling pathway
673 activate gene expression via oxidative post translational modification (oxi-PTM) of different regulatory
674 proteins, yielding a coordinated cellular response to the original stress or signal in the entire colony, biofilm,
675 and/or tissue. Please see text for more details. Abbreviations: oxi-PTM, oxidative post translational
676 modification; ROS, reactive oxygen species.

677 **Table S1.** Rates of the ROS wave in the different experiments.

678 **Figure S1.** Controls for the detection of H_2O_2 on agar plates (in support of Figure 4). Agar plates containing
679 the different growth media used in Figure 4, but without any organisms growing on them, were fumigated
680 with OxyBurst, which detects ROS in the absence of cells. A 1 μL drop of 10 mM or 1 M H_2O_2 was then
681 applied to the plate (indicated with a circle) and whole plate ROS accumulation was imaged for 30 min.
682 Scale bar, 1 cm.

683 **Figure S2.** Representative images of injury inflicted on the H9c2 cell monolayer by a heat-treated metal
684 rod (in support of Figure 7a). Plates with a monolayer of H9c2 cells, used for the experiments shown in
685 Figure 7a were imaged with an Agilent BioTek Lionheart FX automated microscope and the different
686 images collected were assembled to reveal the size of injury inflicted on the monolayer of cells. Scale bar,
687 200 μM.

688 **Figure S3.** Controls for the ability of H9c2 cells that do not show ROS accumulation following the heated
689 rod injury to accumulate ROS (in support of Figure 7). Monolayers of rat cardiomyocytes (H9c2), cells
690 grown in culture were treated or untreated with a heated metal rod (indicated with a circle) to induce injury
691 (average injury diameter is 120 µm) and ROS accumulation was imaged using H_2DCFDA for 60 min in the
692 entire plate. At the end of the 60 min, H_2O_2 at a final concentration of 1 mM was added to the plates and
693 the plates were imaged for an additional 10 min. Representative time-lapse images of whole plate ROS
694 accumulation in treated and untreated plates are shown. Scale bar, 1 cm. Abbreviations: H_2DCFDA, 2',7'-
695 dichlorodihydrofluorescein diacetate; ROS, reactive oxygen species.

696 **Figure S4.** Wound-induced rapid systemic ROS accumulation in hearts from female and male mice. Mice
697 hearts, surgically removed from 9-10-week-old male and female C57BL/6J mice, were untreated, or treated
698 with a heated metal rod (to induce injury), in the presence or absence of DPI (50 µM), and ROS
699 accumulation was measured using H_2DCFDA as described in Figure 8. Bar graphs of combined data from
700 all female **(a)** and male **(b)** hearts used for the analysis at the 0- and 30-min time points are shown (in
701 support of Figure 8). All experiments were repeated at least 3 times with 3 female and 3 male mice per
702 experiment. Data is presented as box plot graphs; X is mean ± S.E., N=30, **$P < 0.01$, ***$P < 0.001$,
703 Student t-test. Scale bar, 1 cm. Female- and male-specific ROS responses are shown in Figure S4.
704 Abbreviations: DPI, diphenyleneiodonium; H_2DCFDA, 2',7'-dichlorodihydrofluorescein diacetate; L, local;
705 ROS, reactive oxygen species; S, systemic; TRE, total radiant efficiency; w/, with.

706 **Movie S1.** A movie showing the ROS signal generated in a monolayer of H9c2 cells following heat injury
707 (in support of Figure 7a). Monolayers of rat cardiomyocytes (H9c2) cells grown in culture were treated
708 with a heated metal rod (indicated with a circle) to induce injury (average injury diameter is 120 µm) and
709 ROS accumulation was imaged using H_2DCFDA in the entire plate. Abbreviations: H_2DCFDA, 2',7'-
710 dichlorodihydrofluorescein diacetate.

711 **Movie S2.** A movie showing the ROS signal generated in an isolated mice heart following heat injury (in
712 support of Figure 8a). Isolated hearts from mice were treated with a heated metal rod (indicated with a
713 circle) to induce injury and ROS accumulation was imaged using H_2DCFDA in the entire plate.
714 Abbreviations: H_2DCFDA, 2',7'-dichlorodihydrofluorescein diacetate.

715

716

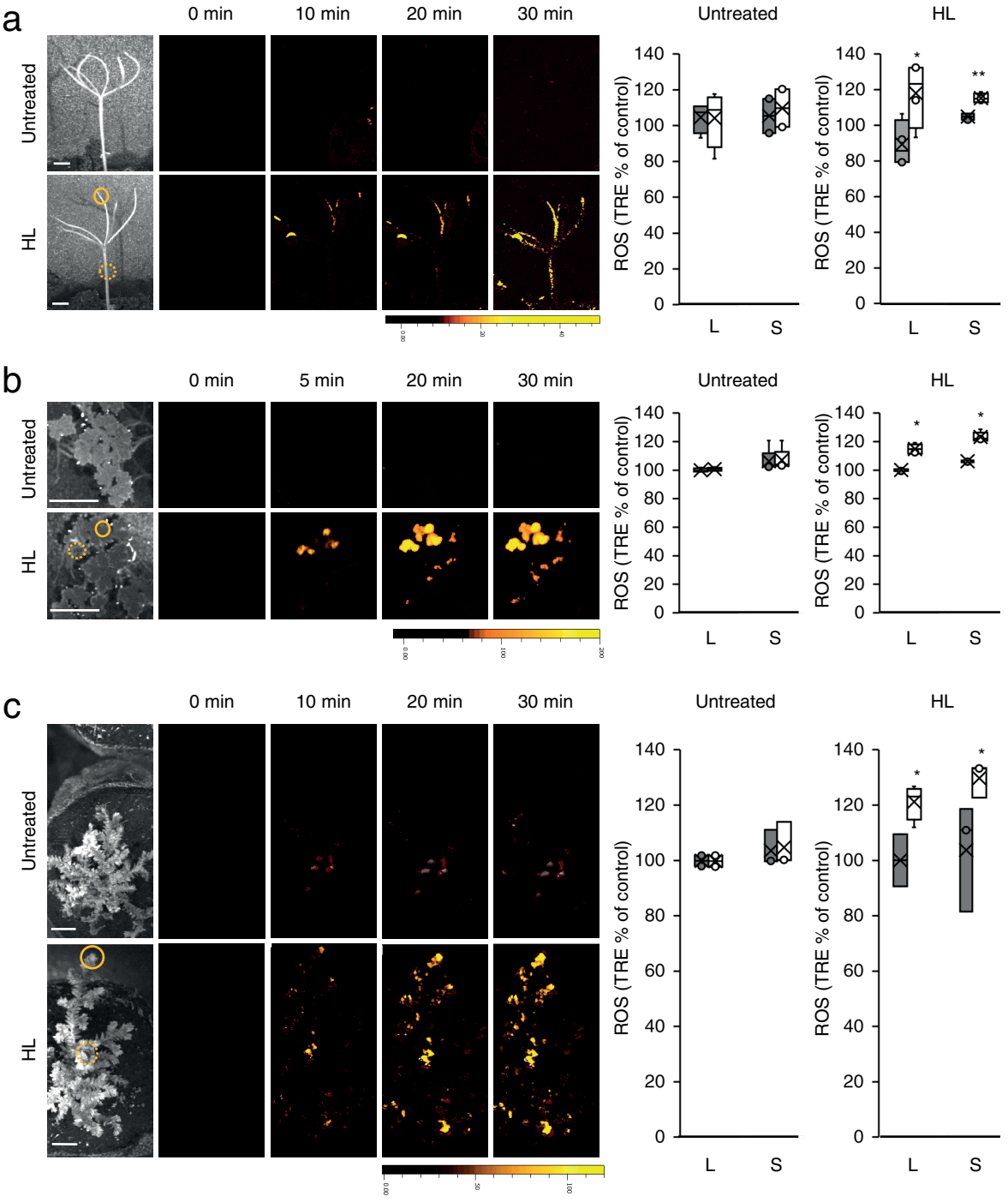

Figure 1. ROS as rapid systemic signals in *Pinus sylvestris*, *Azolla filiculoides*, and *Selaginella moellendorffii.* **(a)** *Pinus sylvestris* plants were subjected to a high light (HL) stress treatment applied to a single leaf, and ROS accumulation was imaged, using H_2DCFDA, in whole plants (local and systemic tissues, indicated with solid and dashed circles, respectively). Representative time-lapse images of whole plant ROS accumulation in treated and untreated *Pinus sylvestris* plants are shown alongside bar graphs of combined data from all plants used for the analysis at the 0- and 30-min time points (local and systemic). **(b)** Same as a but for *Azolla filiculoides*. **(c)** Same as a, but for *Selaginella moellendorffii.* All experiments were repeated at least 3 times with 10 plants per experiment. Data is presented as box plot graphs; X is mean ± S.E., N=30, *P < 0.05, **P < 0.01, Student t-test. Scale bar, 1 cm. Abbreviations: H_2DCFDA, 2',7'-dichlorodihydrofluorescein diacetate; HL, high light; L, local; ROS, reactive oxygen species; S, systemic; TRE, total radiant efficiency.

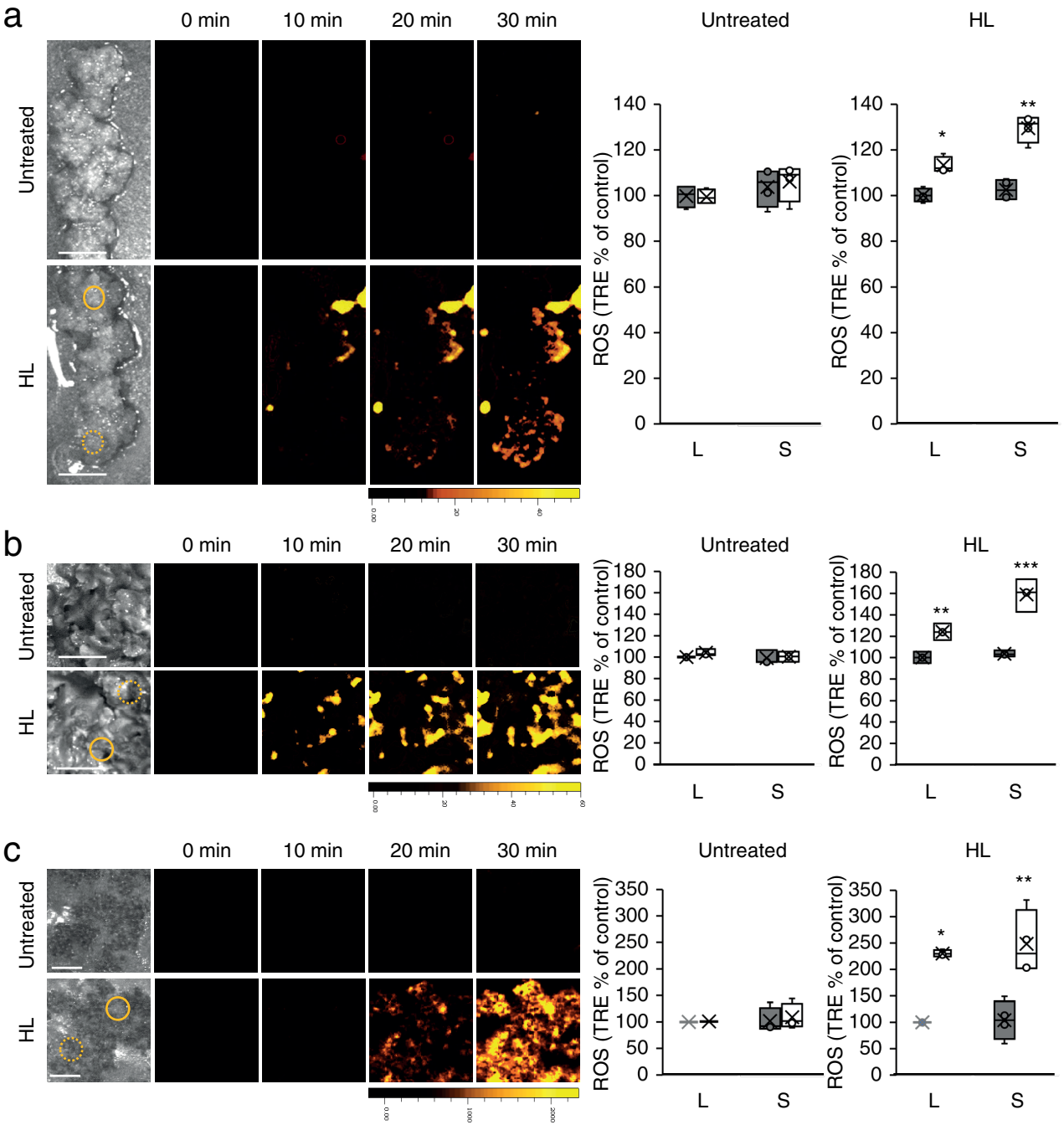

Figure 2. Rapid systemic ROS signaling in non-vascular plants. **(a)** *Anthoceros agrestis* plants were subjected to a high light (HL) stress treatment applied to a single leaf and ROS accumulation was imaged using H_2DCFDA, in whole plants (local and systemic tissues, indicated with solid and dashed circles, respectively). Representative time-lapse images of whole plant ROS accumulation in treated and untreated *Anthoceros agrestis* plants are shown alongside bar graphs of combined data from all plants used for the analysis at the 0- and 30-min time points (local and systemic). **(b)** Same as a but for *Marchantia polymorpha*. **(c)** Same as a, but for *Physcomitrium patens*. All experiments were repeated at least 3 times with 10 plants per experiment. Data is presented as box plot graphs; X is mean ± S.E., N=30, *P < 0.05, **P < 0.01, ***P < 0.001, Student t-test. Scale bar, 1 cm. Abbreviations: H_2DCFDA, 2',7'-dichlorodihydrofluorescein diacetate; HL, high light; L, local; ROS, reactive oxygen species; S, systemic; TRE, total radiant efficiency.

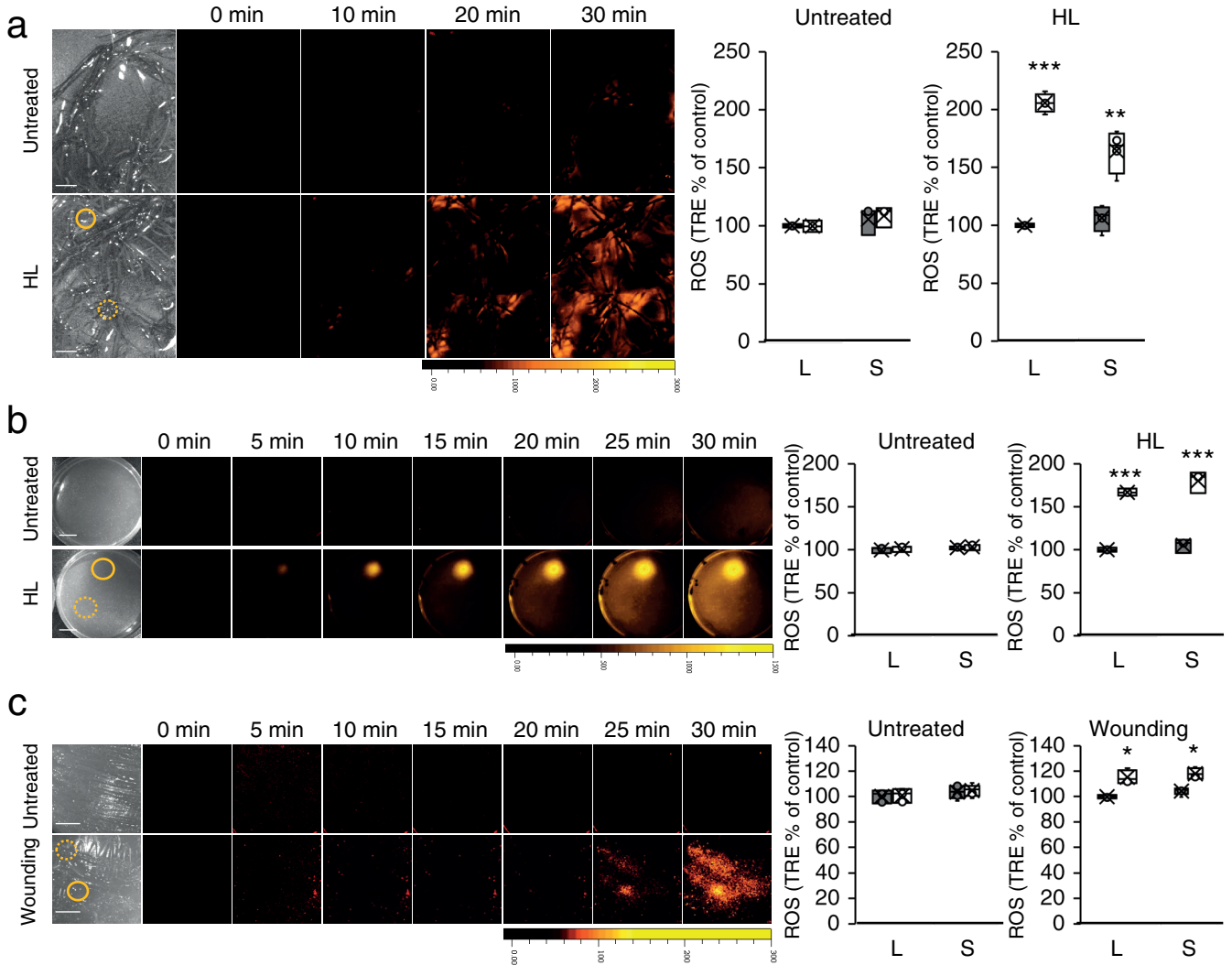

Figure 3. Rapid systemic ROS signaling in multicellular algae and unicellular organisms. **(a)** *Chara vulgaris*, a multicellular alga, was subjected to a high light (HL) stress treatment applied to a single branch, and ROS accumulation was imaged, using H_2DCFDA, in several branches of the alga (local and systemic tissues, indicated with solid and dashed circles, respectively). Representative time-lapse images of whole alga ROS accumulation in treated and untreated *Chara vulgaris* are shown alongside bar graphs of combined data from all plants used for the analysis at the 0- and 30-min time points (local and systemic). **(b)** An agar plate containing a lawn of *Chlamydomonas reinhardtii*, a unicellular alga, was treated with a focused beam of HL (local treatment), and ROS accumulation was imaged, using H_2DCFDA, in the entire plate (local and systemic tissues are indicated with solid and dashed circles, respectively). Representative time-lapse images of whole plate ROS accumulation of treated and untreated *Chlamydomonas* lawn are shown alongside bar graphs of combined data from all plants used for the analysis at the 0- and 30-min time points (local and systemic). **(c)** Same as in b, but for an agar plate that contains a lawn of *Dictyostelium discoideum* that was treated locally with a heated rod (local). All experiments were repeated at least 3 times with 10 multicellular alga, or agar plates per experiment. Data is presented as box plot graphs; X is mean ± S.E., N=30, *P < 0.05, **P < 0.01, ***P < 0.001, Student t-test. Scale bar, 1 cm. Abbreviations: H_2DCFDA, 2',7'-dichlorodihydrofluorescein diacetate; HL, high light; L, local; ROS, reactive oxygen species; S, systemic; TRE, total radiant efficiency.

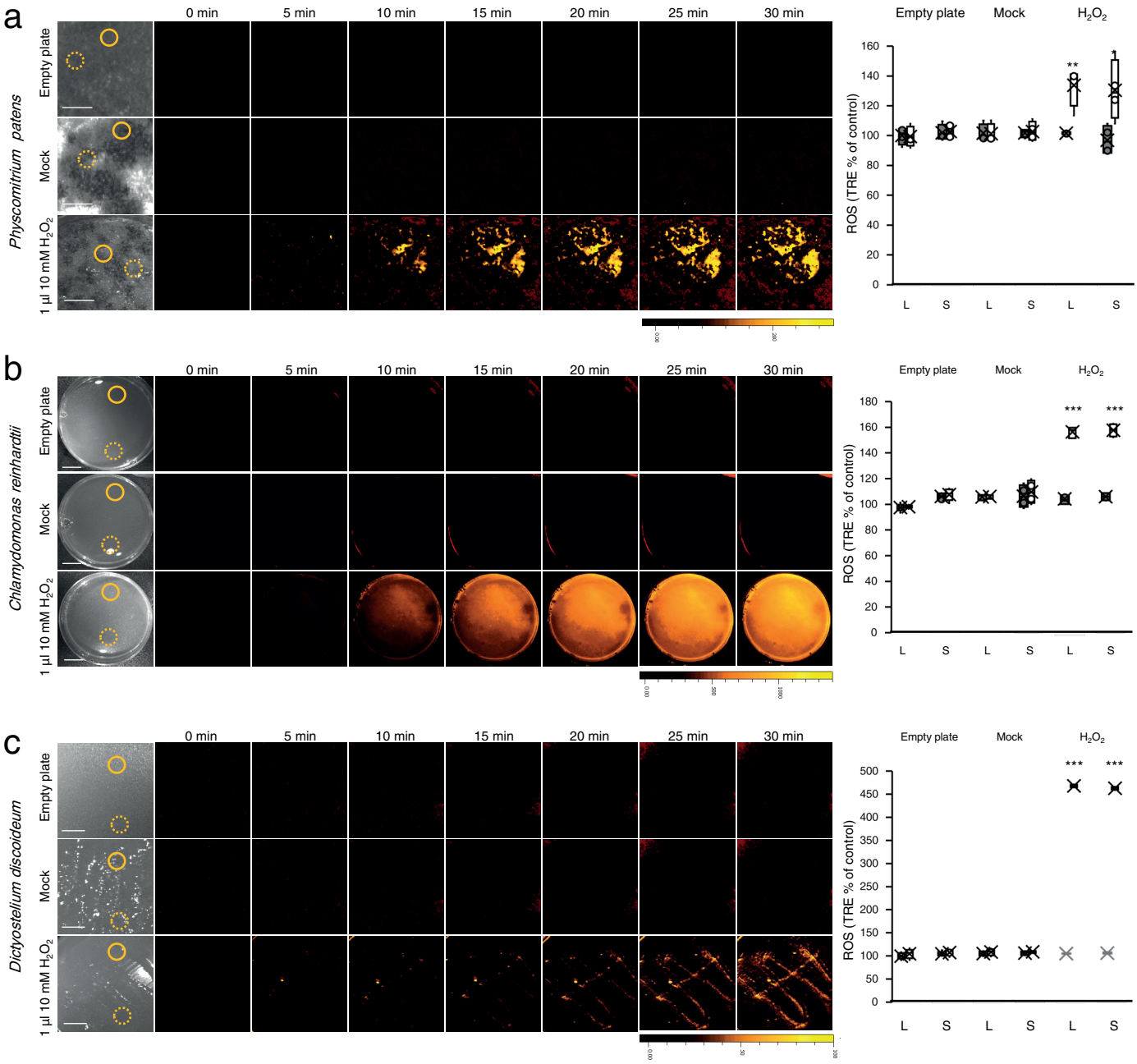

Figure 4. Activation of the rapid systemic ROS signal in *Physcomitrium patens*, *Chlamydomonas reinhardtii*, and *Dictyostelium discoideum* by a local application of H_2O_2. **(a)** An agar plate without *Physcomitrium patens* (top), and agar plates with a lawn of *Physcomitrium patens* (middle and bottom), were treated with 1 µl of 1 mM H_20_2 (top and bottom), or 1 µl of media (mock, middle), and ROS accumulation was imaged using H_2DCFDA in the entire plate. Representative time-lapse images of whole plate ROS accumulation are shown alongside bar graphs of combined data from all plates used for the analysis at the 0- and 30-min time points (local and systemic). Local and systemic sampling locations are indicated with solid and dashed circles, respectively. **(b)** Same as a, but for plates with or without a lawn of *Chlamydomonas reinhardtii*. **(c)** Same as in a, but for plates with or without *Dictyostelium discoideum*. All experiments were repeated at least 3 times with 10 agar plates per experiment. Data is presented as box plot graphs; X is mean ± S.E., N=30, *P < 0.05, **P < 0.01, ***P < 0.001, Student t-test. Scale bar, 1 cm. Abbreviations: H_2DCFDA, 2',7'-dichlorodihydrofluorescein diacetate; HL, high light; L, local; ROS, reactive oxygen species; S, systemic; TRE, total radiant efficiency.

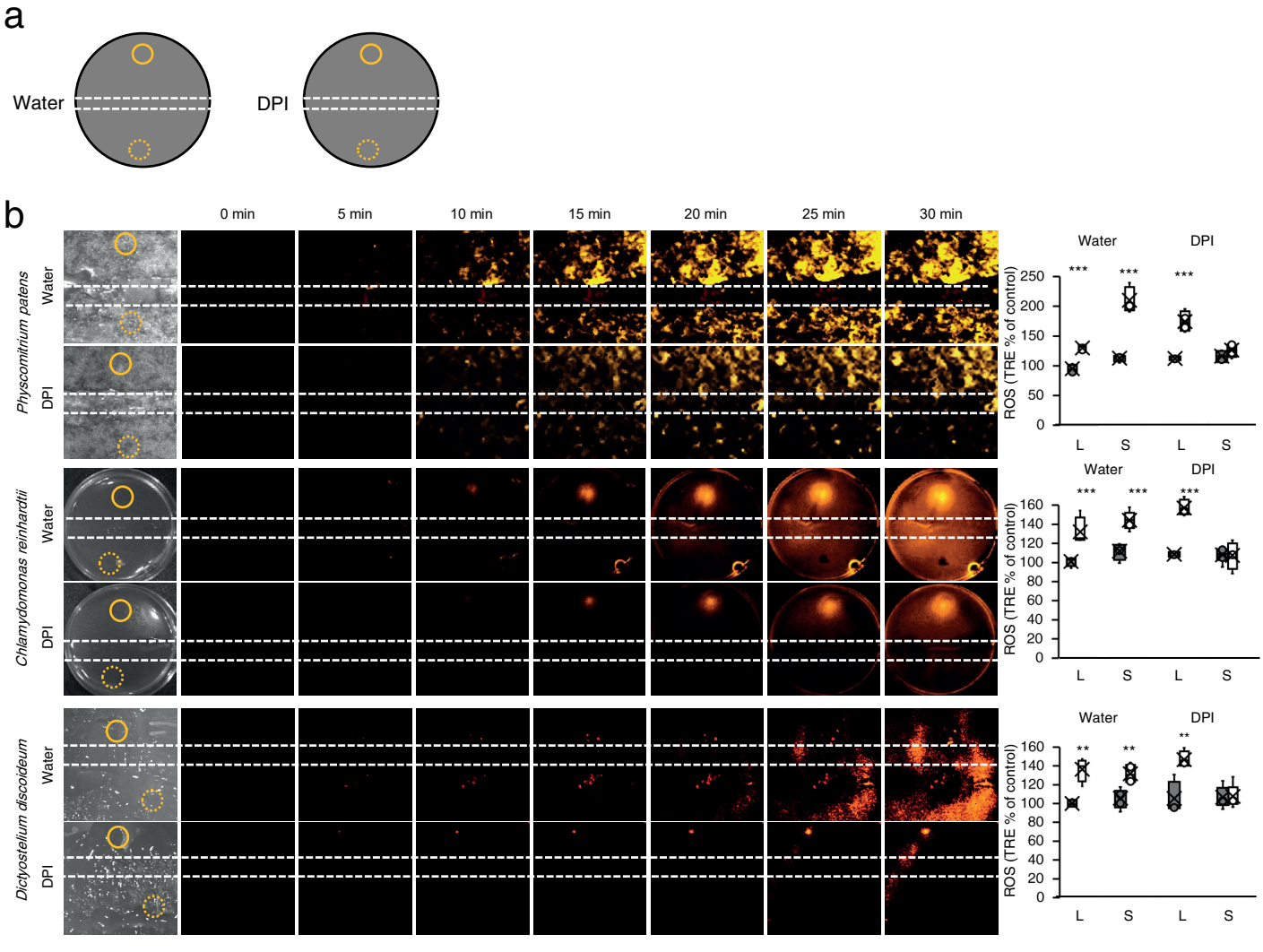

Figure 5. Inhibition of the rapid systemic ROS signal in *Physcomitrium patens*, *Chlamydomonas reinhardtii*, and *Dictyostelium discoideum* by DPI. **(a)** A diagram showing the experimental design used. A strip of agar containing water or the NOX/RBOH inhibitor DPI (50 µM) was layered over the middle of agar plates containing a lawn of the different organisms growing on them. Following a 5 min incubation one side of the plate was treated with a focused beam of high light (HL) or touched with a heated rod (local) and ROS accumulation was imaged using H_2DCFDA in the entire plate. Local and systemic locations used for signal quantification are indicated with solid and dashed circles, respectively. **(b)** Representative time-lapse images of whole plate ROS accumulation are shown alongside bar graphs of combined data from all plates used for the analysis at the 0- and 30-min time points (Water or DPI treated *Physcomitrium patens*, *Chlamydomonas reinhardtii*, or *Dictyostelium discoideum*; top, middle, and bottom, respectively; local and systemic). All experiments were repeated at least 3 times with 10 agar plates per experiment. Data is presented as box plot graphs; X is mean ± S.E., N=30, **P < 0.01, ***P < 0.001, Student t-test. Scale bar, 1 cm. Abbreviations: DPI, diphenyleneiodonium; H_2DCFDA, 2',7'-dichlorodihydrofluorescein diacetate; HL, high light; L, local; NOX, NADPH oxidase; RBOH, respiratory burst oxidase homolog; ROS, reactive oxygen species; S, systemic; TRE, total radiant efficiency.

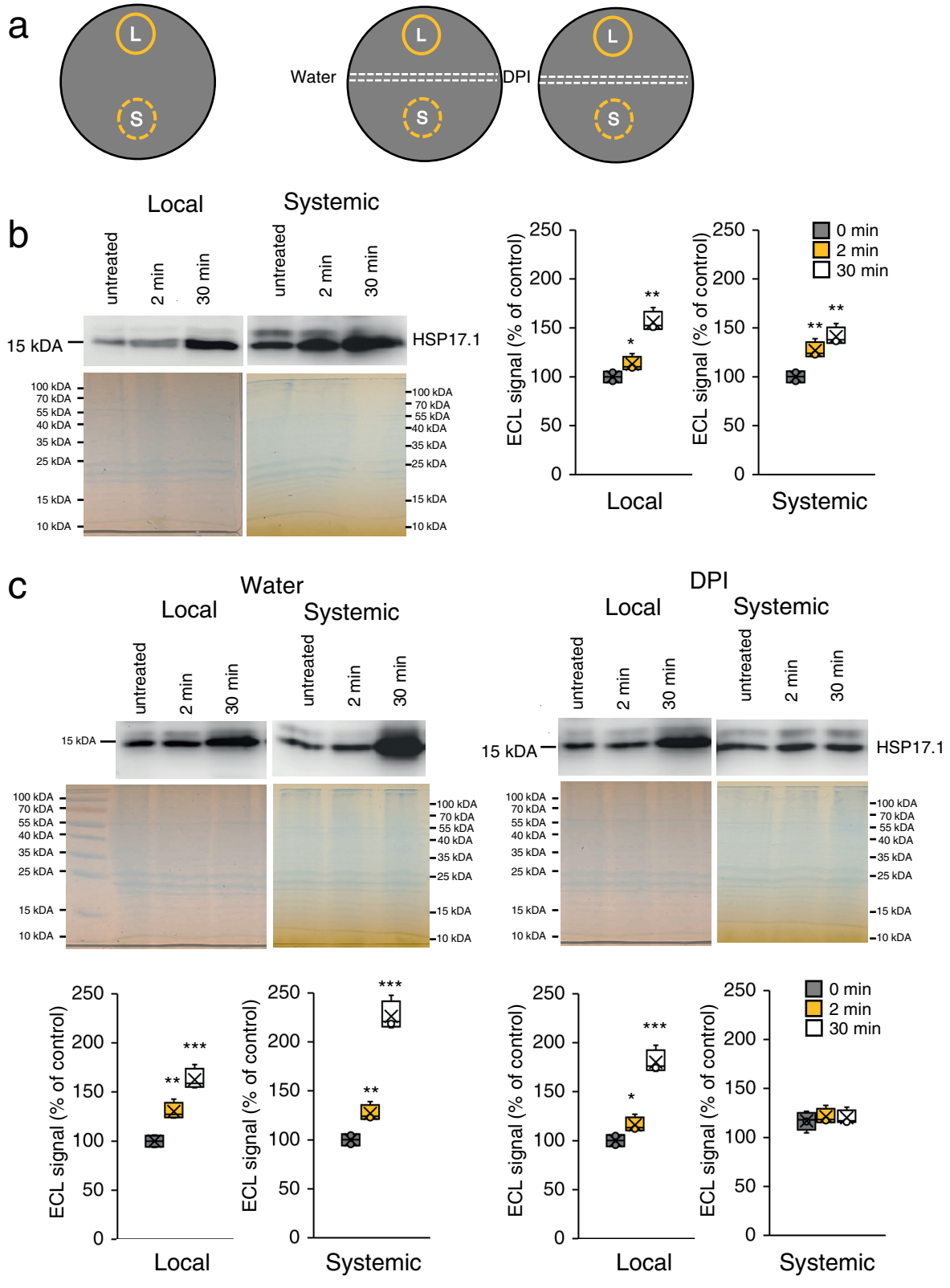

Figure 6. Functional analysis of the cell-to-cell rapid ROS signal in *Chlamydomonas reinhardtii*. **(a)** Diagrams showing the experimental designs used. Left: A lawn of *Chlamydomonas reinhardtii* growing on an agar plate was subjected to a focused beam of high light (HL) stress and the area subjected to the beam (local, L), as well as an area that is on the other end of the plate (systemic, S) were sampled at different times following the application of HL for analysis of the expression of the light stress response small heat shock protein 17.1 (sHSP17.1; This design was used for the experiments shown in b). Right: A strip of agar containing water or the NOX/RBOH inhibitor DPI (50 µM) was layered over the middle of agar plates containing the lawn of *Chlamydomonas reinhardtii* 5 min prior to the application of light stress and sampling (This design was used for the experiments shown in c). Local and systemic sampling locations are indicated with solid and dashed circles, respectively. **(b)** Representative protein blots and Coomassie- stained gels are shown alongside bar graphs of combined data from all blots used for the analysis at the 0-, 2-, and 30-min time points, for the expression of sHSP17.1 in the L and S locations, following the light stress treatment. **(c)** Same as in b, but for experiments in which a strip of agar containing water (left) or DPI (right) was layered over the middle of agar plates 5 min prior to the application of HL stress. All experiments were repeated at least 3 times with 10 agar plates per experiment. Data is presented as box plot graphs; X is mean ± S.E., N=30, *P < 0.05, **P < 0.01, ***P < 0.001, Student t-test. Abbreviations: DPI, diphenyleneiodonium; ECL, enhanced chemiluminescence; H_2DCFDA, 2',7'-dichlorodihydrofluorescein diacetate; HL, high light; L, local; NOX, NADPH oxidase; RBOH, respiratory burst oxidase homolog; ROS, reactive oxygen species; S, systemic; sHSP, small heat shock protein 17.1.

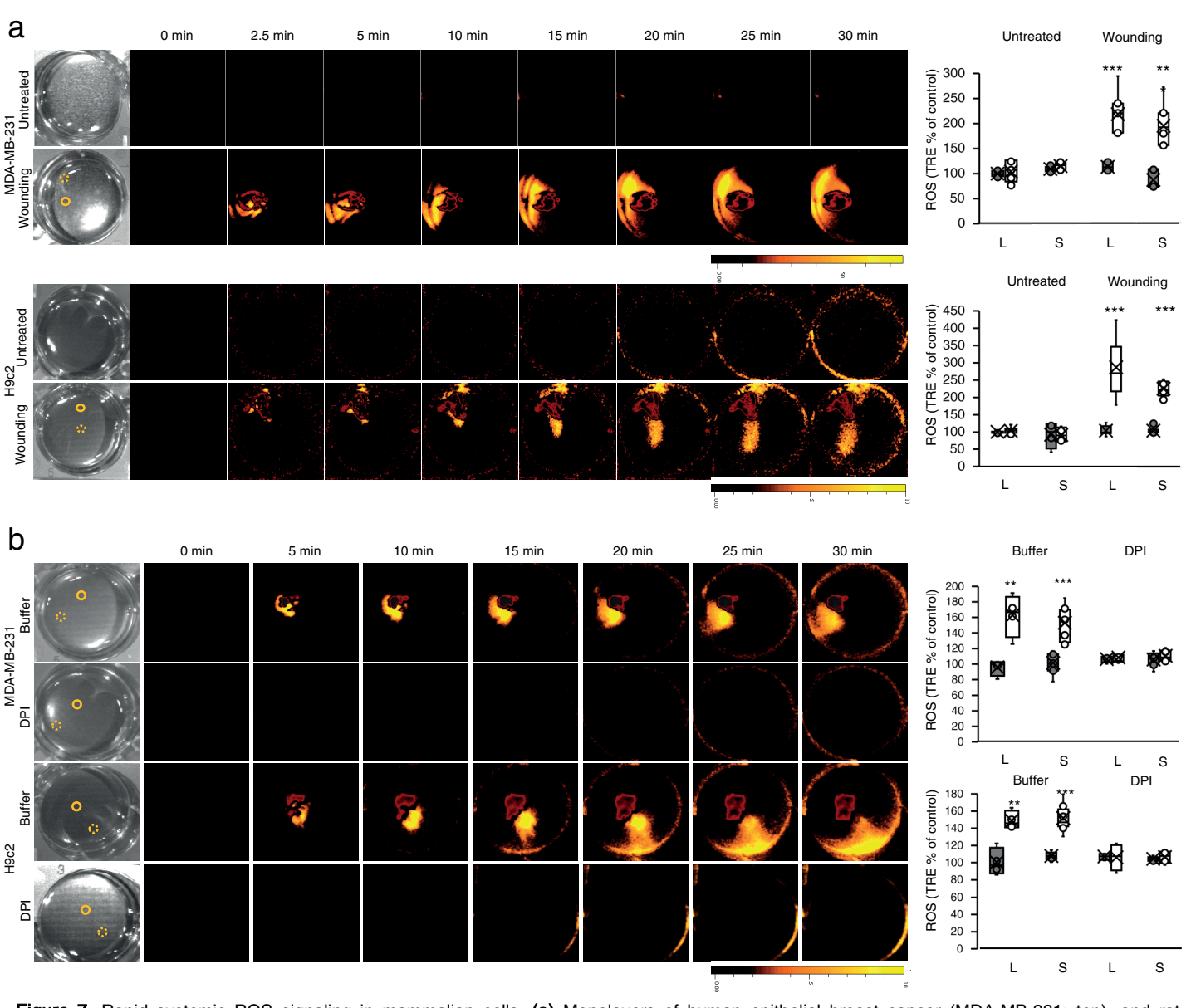

Figure 7. Rapid systemic ROS signaling in mammalian cells. **(a)** Monolayers of human epithelial breast cancer (MDA-MB-231; top), and rat cardiomyocytes (H9c2; bottom), cells grown in culture were treated with a heated metal rod to induce injury (average injury diameter is 120 µm) and ROS accumulation was imaged using H_2DCFDA in the entire plate. Representative time-lapse images of whole plate ROS accumulation in treated and untreated plates are shown alongside bar graphs of combined data from all plates used for the analysis at the 0- and 30-min time points (local and systemic). Local and systemic sampling locations are indicated with solid and dashed circles, respectively. **(b)** Same as in a, except that buffer or DPI (50 µM) were added to the growth media of cells 10 min prior to the heat injury. All experiments were repeated at least 3 times with 10 agar plates per experiment. Data is presented as box plot graphs; X is mean ± S.E., N=30, **P < 0.01, ***P < 0.001, Student t-test. Scale bar, 1 cm. Abbreviations: DPI, diphenyleneiodonium; H_2DCFDA, 2',7'-dichlorodihydrofluorescein diacetate; L, local; ROS, reactive oxygen species; S, systemic; TRE, total radiant efficiency.

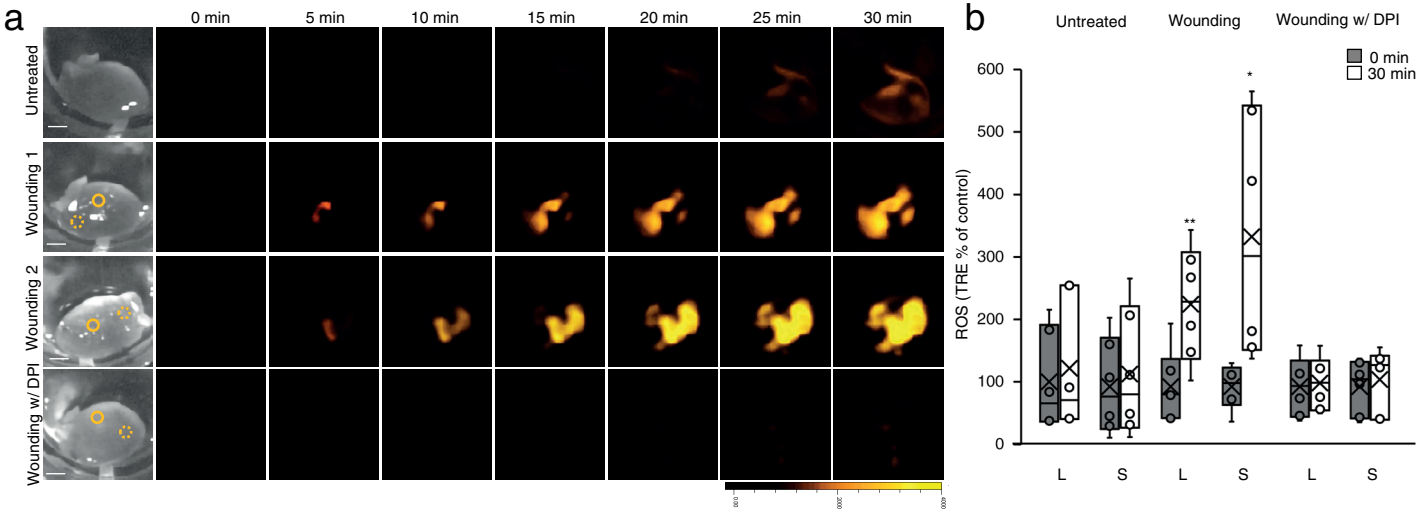

Figure 8. Wound-induced rapid systemic ROS signaling in isolated mice hearts. Mice hearts, surgically removed from 9-10-week-old male and female C57BL/6J mice, were untreated, or treated with a heated metal rod (to induce injury), in the presence or absence of DPI (50 μM), and ROS accumulation was imaged using H_2DCFDA in the entire hearts. Representative time-lapse images of whole heart ROS accumulation **(a)** are shown alongside bar graphs of combined data from all hearts used for the analysis at the 0- and 30-min time points **(b)**. Local and systemic sampling locations are indicated with solid and dashed circles, respectively. All experiments were repeated at least 3 times with 3 female and 3 male mice per experiment. Data is presented as box plot graphs; X is mean ± S.E., N=30, **P < 0.01, ***P < 0.001, Student t-test. Scale bar, 1 cm. Scale bar is 0.1cm. Female- and male-specific ROS responses are shown in Figure S4. Abbreviations: DPI, diphenyleneiodonium; H_2DCFDA, 2',7'-dichlorodihydrofluorescein diacetate; L, local; ROS, reactive oxygen species; S, systemic; TRE, total radiant efficiency; w/, with.

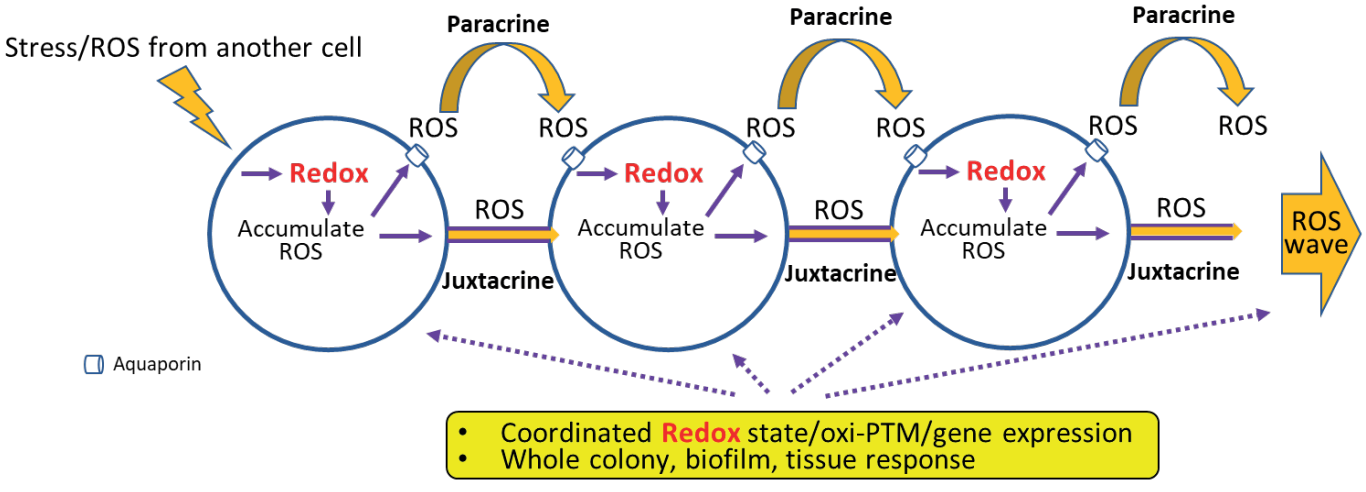

Figure 9. A model depicting the principle of the cell-to-cell ROS signaling pathway that is conserved between unicellular and multicellular organisms. An initiating cell that perceives a stress or ROS signal is shown on the left to undergo a change in redox levels that will cause the accumulation of ROS in that cell. This process is shown to cause the activation of a paracrine and juxtacrine ROS-mediated cell-to-cell signal transduction pathway. Each cell along the path of this pathway accumulates ROS maintaining the signal and transmitting it to the next. The resulting changes in redox in all cells involved in this signaling pathway activate gene expression via oxidative post translational modification (oxi-PTM) of different regulatory proteins, yielding a coordinated cellular response to the original stress or signal in the entire colony, biofilm, and/or tissue. Please see text for more details. Abbreviations: oxi-PTM, oxidative post translational modification; ROS, reactive oxygen species.

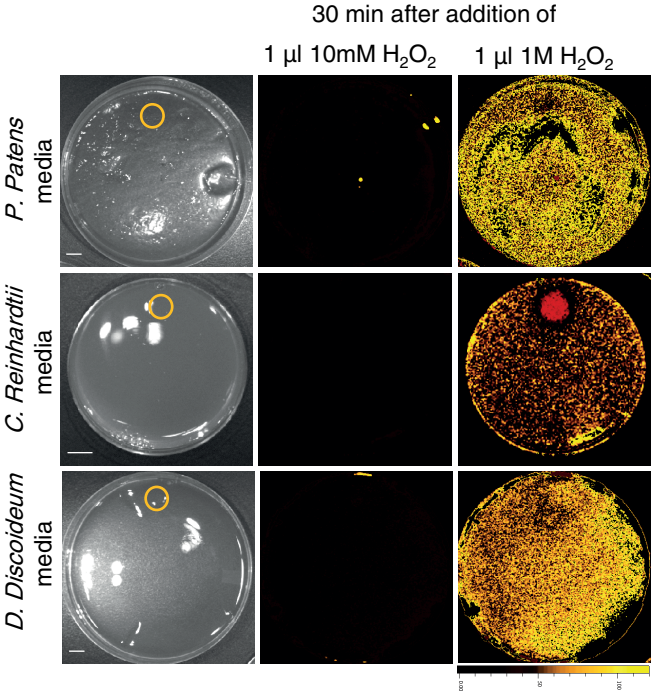

Figure S1. Controls for the detection of H_2O_2 on agar plates (in support of Figure 4). Agar plates containing the different growth media used in Figure 4, but without any organisms growing on them, were fumigated with OxyBurst, which detects ROS in the absence of cells. A 1 µL drop of 10 mM or 1 M H_2O_2 was then applied to the plate (indicated with a circle) and whole plate ROS accumulation was imaged for 30 min. Scale bar, 1 cm.

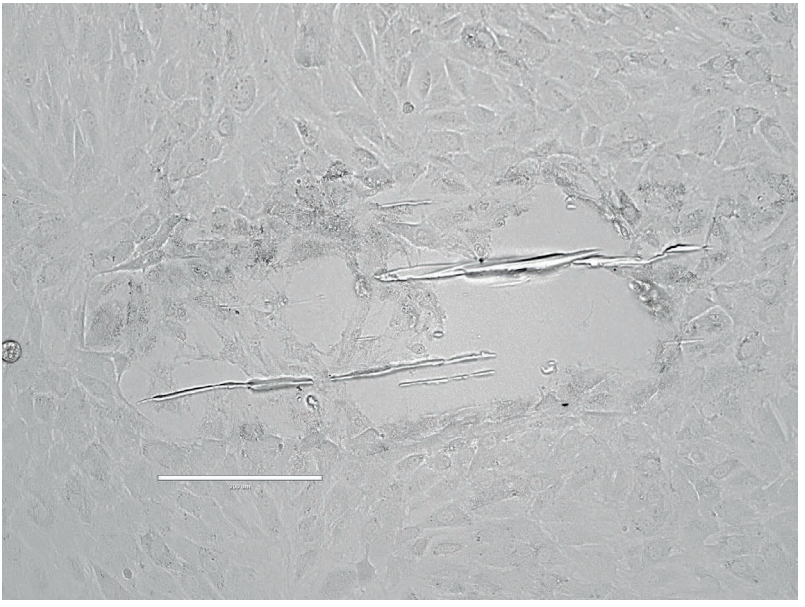

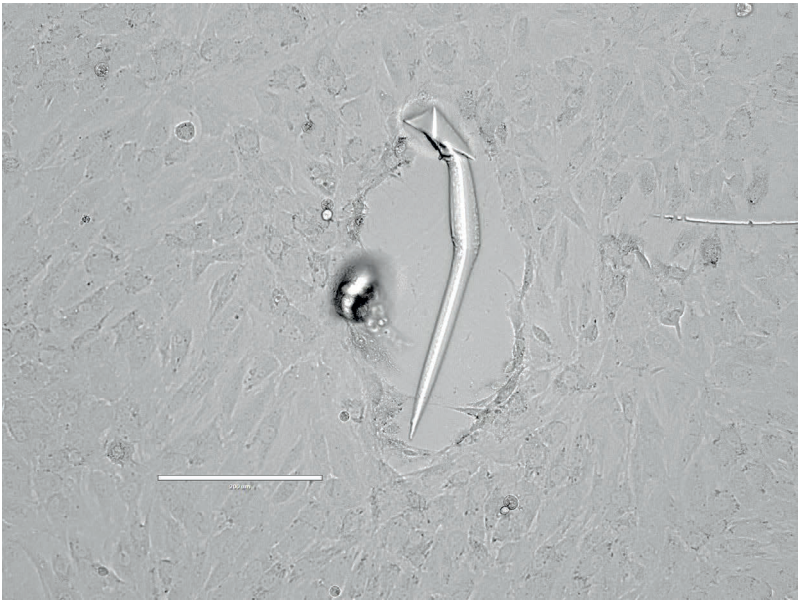

Figure S2. Representative images of injury inflicted on the H9c2 cell monolayer by a heat-treated metal rod (in support of Figure 7a). Plates with a monolayer of H9c2 cells, used for the experiments shown in Figure 7a were imaged with an Agilent BioTek Lionheart FX automated microscope and the different images collected were assembled to reveal the size of injury inflicted on the monolayer of cells. Scale bar, 200 μM.

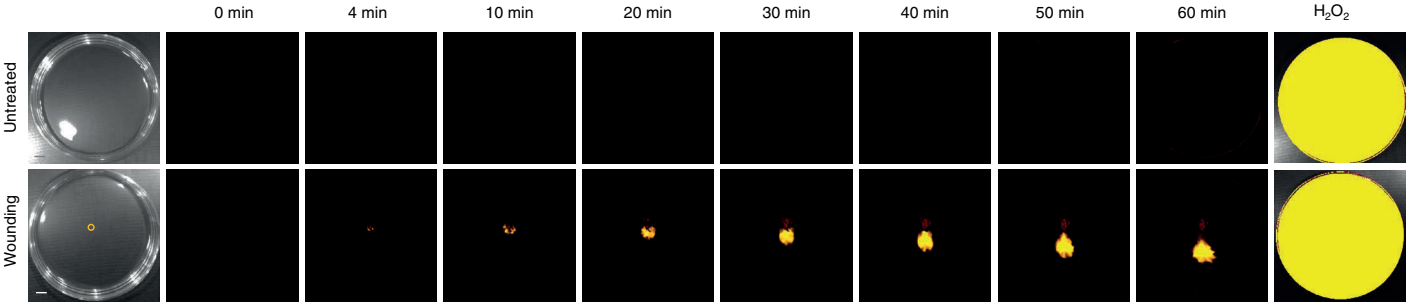

Figure S3. Controls for the ability of H9c2 cells that do not show ROS accumulation following the heated rod injury to accumulate ROS (in support of Figure 7). Monolayers of rat cardiomyocytes (H9c2), cells grown in culture were treated or untreated with a heated metal rod (indicated with a circle) to induce injury (average injury diameter is 120 µm) and ROS accumulation was imaged using H_2DCFDA for 60 min in the entire plate. At the end of the 60 min, H_2O_2 at a final concentration of 1 mM was added to the plates and the plates were imaged for an additional 10 min. Representative time-lapse images of whole plate ROS accumulation in treated and untreated plates are shown. Scale bar, 1 cm. Abbreviations: H_2DCFDA, 2',7'-dichlorodihydrofluorescein diacetate; ROS, reactive oxygen species.

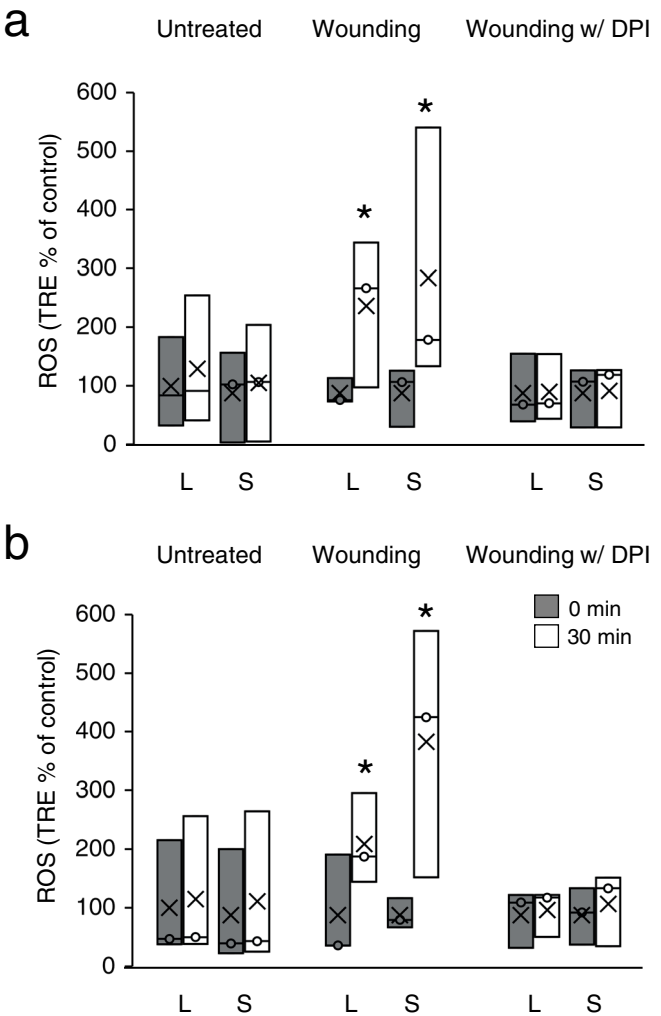

Figure S4. Wound-induced rapid systemic ROS accumulation in hearts from female and male mice. Mice hearts, surgically removed from 9-10-week-old male and female C57BL/6J mice, were untreated, or treated with a heated metal rod (to induce injury), in the presence or absence of DPI (50 μM), and ROS accumulation was measured using H_2DCFDA as described in Figure 8. Bar graphs of combined data from all female **(a)** and male **(b)** hearts used for the analysis at the 0- and 30-min time points are shown (in support of Figure 8). All experiments were repeated at least 3 times with 3 female and 3 male mice per experiment. Data is presented as box plot graphs; X is mean ± S.E., N=30, $^{**}P < 0.01$, $^{***}P < 0.001$, Student t-test. Scale bar, 1 cm. Abbreviations: DPI, diphenyleneiodonium; H_2DCFDA, 2',7'-dichlorodihydrofluorescein diacetate; L, local; ROS, reactive oxygen species; S, systemic; TRE, total radiant efficiency; w/, with.

Table S1 – Rates of the ROS wave in the different experiments

Figure	**description**	**rate (cm min^{-1})**	**Treatment**
1A	*Pinus sylvestris*	0.18	HL
1B	*Azolla filiculoides*	0.1	
1C	*Selaginella moellendorffii*	0.14	
Fig 1	**Average**	0.14	
2A	*Anthoceros agrestis*	0.11	
2B	*Marchantia polymorpha*	0.12	
2C	*Physcomitrium patens*	0.17	
Fig 2	**Average**	0.13	
3A	*Chara*	0.14	
3B	*C. reinhardtii*	0.12	
3C	*D. discoideum*	0.2	Wounding
Fig 3	**Average**	0.15	
Fig 4	*D. discoideum*	0.09	H_2O_2
Fig 4	*C. reinhardtii*	0.12	
Fig 4	*Physcomitrium patens*	0.11	
Fig 4	**Average**	0.107	
7A	MDA-MB-231	0.288	Wounding
7A	H9c2	0.203	
Fig 7	**Average**	0.245	
Fig 8	*Mus musculus* hearts	0.112	Wounding